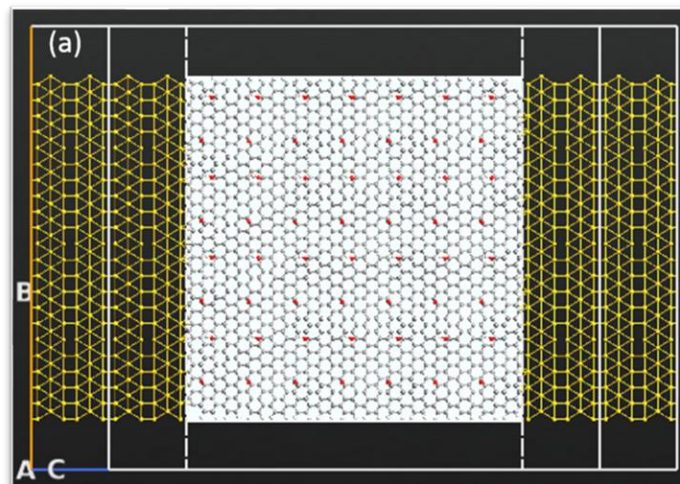**MASTER THESIS NO. 2022: 88**

College of Engineering

Department of Electrical and Communication Engineering

THE DESIGN OF A POINT OF CARE FET BIOSENSOR TO DETECT AND SCREEN COVID-19

Nisreen Amer Mohammad Alnaji

November 2022

United Arab Emirates University

College of Engineering

Department of Electrical and Communication Engineering

THE DESIGN OF A POINT OF CARE FET BIOSENSOR TO
DETECT AND SCREEN COVID-19

Nisreen Amer Alnaji

This thesis is submitted in partial fulfilment of the requirements for the degree of Master
of Science in Electrical Engineering

November 2022

Cover: The designed FET biosensor

(Photo: By Nisreen Amer Alnaji)

Declaration of Original Work

I, Nisreen Amer Alnaji, the undersigned, a graduate student at the United Arab Emirates University (UAEU), and the author of this thesis entitled "*The Design of a Point of Care FET biosensor to Detect and Screen COVID-19*", hereby, solemnly declare that this is the original research work done by me under the supervision of Prof. Falah Awwad, in the College of Engineering at UAEU. This work has not previously formed the basis for the award of any academic degree, diploma or a similar title at this or any other university. Any materials borrowed from other sources (whether published or unpublished) and relied upon or included in my thesis have been properly cited and acknowledged in accordance with appropriate academic conventions. I further declare that there is no potential conflict of interest with respect to the research, data collection, authorship, presentation and/or publication of this thesis.

Student's Signature:

Date: 17th November 2022

Approval of the Master Thesis

This Master Thesis is approved by the following Examining Committee Members:

1) Advisor (Committee Chair): Falah Awwad
   Title: Professor
   Department of Electrical and Communication Engineering
   College of Engineering

   Signature: _____   Date 14/Dec/2022

2) Member: Mohammad Hayajneh
    Title: Associate Professor
    Department of Computer & Network Engineering
    College of Information Technology

   Signature: _Mohammad Hayajneh_ _____   Date 14/Dec/2022

3) Member (External Examiner): Baker Mohammad
   Title: Professor
   Department of Electrical Engineering and Computer Science
   Institution: Khalifa University, UAE

   Signature: _____   Date 14/Dec/2022

This Master Thesis is accepted by:

Acting Dean of the College of Engineering: Professor Mohamed H. Al-Marzouqi

Signature _Mohamed AlMarzouqi_

Date _Jan. 18, 2023_

Dean of the College of Graduate Studies: Professor Ali Al-Marzouqi

Signature _Ali Hassan_

Date _18/01/2023_

Abstract

This work proposes and demonstrates a biosensor with reduced Graphene Oxide (rGO) based Field Effect Transistor (FET) for rapid and selective detection of Severe Acute Respiratory Syndrome Coronavirus 2 (SARS-CoV-2). The main objective of this thesis is to detect the SARS-CoV-2 spike protein antigen on spot selectively and rapidly. The rGO channel is coated with the spike protein antibodies to achieve selectivity. Moreover, the biosensing performance and specificity are governed by decorating the sensor's channel with Metal Nanoparticles (MNPs) such as, copper, and silver. The designed sensor successfully detects the SARS-CoV-2 spike protein and shows singular electrical behavior for detection. The rGO-FET biosensor electronic transport characteristics such as transmission spectrum, electronic current, and transfer curves are studied by using semiempirical modeling combined with a nonequilibrium Green's function. The transmission spectrum, I-V and transfer curves are investigated to spot the performance alteration caused by detecting the target molecule. The sensor is also tested against another virus, namely Rabies virus, and showed no detection reaction towards it. The introduced sensor is 8.2 nm long and 6.1 nm wide which makes it a perfect candidate for easy handling and transporting. RGO FET-based biosensor is developed and tested to take the advantage of the unique electronic properties of the rGO channel and offer a quick, rapid, easy, and accurate detection method for SARS-CoV-2 virus. The semiempirical study, along with the simulations results are in agreement with the previous literature studies and provide an excellent pathway for practical fabrication.

Keywords: Semiempirical, FET, rGO, MNPs, biosensor, COVID-19, SARS-CoV-2.

Title and Abstract (in Arabic)

تصميم مستشعر باستخدام ترانزستور مجاليّ التأثير لرصد و ضبط فيروس كورونا (كوفيد-19) عند نقاط الرعاية الصحية

الملخص

تتناول هذه الأطروحة دراسة الخصائص الإلكترونية والنمذجة الشبه تجريبية (Semi-empirical modelling) لمستشعر بني باستخدام ترانزستور مجاليّ التأثير (Field Effect Transistor) من مادة الجرافين المؤكسد (rGO) لرصد فيروس كورونا المستجد (SARS-CoV-2) عند نقاط الرعاية الصحية. الهدف الرئيسي لهذا العمل هو الرصد الدقيق والضبط السريع لفيروس كورونا، حيث سيتم الاستشعار بوجود الفيروس من خلال بروتين خاص يعرف بـ Spike protein. القناة المصنوعة من الجرافين المؤكسد سوف تغطى وتعالج بأجسام مضادة مخصصة للكشف عن هذا البروتين، ستساعد هذه الخطوة في تحقيق الدقة المطلوبة بينما استعمال وإضافة الجزيئات المعدنية (MNPs) مثل الفضة والنحاس سيعمل على تجهيز السطح للكشف البيولوجي وتعزيز الدقة. المستشعر المصمم سوف يكشف بنجاح عن وجود فيروس كورونا من عدمه في العينة، وأيضاً سوف يظهر رد فعل كهربائي مميز كعلامة على كشفه. في هذا البحث سوف ندرس الطيف الانتقالي (transmission spectrum) ومنحنيات الأداء مثل الـ (I-V curve) لتحديد التغيير المحدث عند ضبط هذا البروتين. إضافة لذلك، لقد تم فحص دقة المستشعر باستخدام فيروس آخر (Rabies virus) ولم يظهر أي ردة فعل استشعارية نحوه. طول المستشعر 8.2 نانومتر وعرضه 6.1 نانومتر ولذلك فهو مثالي للنقل السريع والتعامل السهل. لقد صممنا مستشعر باستخدام ترانزستور مجاليّ التأثير والذي يستفيد من الصفات المميزة للجرافين المؤكسد ويقدّم ضبط دقيق، سريع وسهل لفيروس كورونا المستجد. نتائج الدراسة الشبه تجريبية والنتائج المستخرجة من المحاكاة باستخدام برنامج التصميم متطابقات إلى حد كبير مع البحوث السابقة في هذا المجال وتوفر دليل مناسب لصنع هذه المستشعرات الدقيقة.

مفاهيم البحث الرئيسية: ترانزستور مجاليّ التأثير، الجرافين المؤكسد، فيورس كورونا المستجد، نمذجة شبه تجريبية، ذرات معدنية، فيروس كورونا، مستشعر أحيائيّ.

Acknowledgements

All thanks and praise to Almighty Allah for all the gifts and opportunities he granted to me along my journey in life.

Also, no words can express how grateful I am toward my advisor and role model Prof. Falah Awwad, he was the person who encouraged and supported me during these years and the main reason I loved and enjoyed this area of study. Moreover, thanks go to all the committee members for their continuous efforts.

Finally, I would like to thank my parents, husband, sisters, and my friend Dr. Asma Wasfi for being there when I needed support and encouragement.

Dedication

To my beloved parents, husband, son, sisters and friends.

Table of Contents

List of Tables

List of Figures

List of Abbreviations

AI	Artificial Intelligence
CNP	Charge Neutrality Point
CT	Computed Tomography
DFT	Density Functional Theory
EH	Extended Huckle
Ef	Fermi Level
ELISA	Enzyme Linked Immunosorbent Assay
FET	Field Effect Transistor
GGO	Ground Glass Opacity
LOD	Limit of Detection
MC	Metal Contact
NDR	Negative Differential Resistance
NEGF	Non-Equilibrium Green's Function
rGO	Reduced Graphene Oxide
RT-PCR	Reverse Transcription-Polymerase Chain Reaction
SARS-CoV-2	Severe Acute Respiratory Syndrome Coronavirus 2
SC	Self-Consistent
SE	Semi-Empirical
SERS	Surface Enhanced Raman Scattering

Chapter 1: Introduction

1.1 Overview

Viral pandemics have always been one of the most feared events to occur due to their huge impacts on our mental and physical health, economy, education, and even social lives. Spread area, symptoms, incubation period, rapid and accurate infection detection, therapeutics, and disease's severity are the key factors to be focused on when trying to control such pandemics. Since the identification and spread of SARS-CoV-2 our lives have changed, it's now the ultimate goal for many researchers and medical field staff to find the needed tools to detect, contain, treat and even vaccinate against the viral infection.

1.2 Statement of the Problem

With the recent spread of the new emerging Coronavirus disease 2019 (COVID-19) and due to its highly contagious nature, World Health Organization (WHO) has announced it as a worldwide pandemic. Owing to this, the need for rapid, accurate, and point-of-care detection and screening tools is arising. Until now many detection tools have been proposed in this matter however, none has been approved or confirmed to introduce the best performance in terms of sensitivity, accuracy, and speed. Hence in this work, a point-of-care Field Effect Transistor (FET)-based biosensor will be simulated and studied to serve this matter.

1.3 Research Objectives

This research aims to develop a point-of-care rapid and accurate SARS-CoV-2 sensor. The sensor's electrical properties such as transmission spectrum and electrical current will be studied and analyzed to provide a comprehensive understanding of the sensor's working principles.

Also, it is the purpose of this work to participate and introduce solutions to worldwide pandemics, it is with these intentions in mind the idea of this study was originated.

1.4 Thesis Organization

Chapter 1 introduces a general overview, problem statement, research objectives and thesis outline.

In Chapter 2 the literature which is related to this study is discussed and presented as follows, COVID-19 pandemic, virus structure, SARS-CoV-2 detection techniques, biosensors for viral detection, biosensors for SARS-CoV-2 detection, graphene, bandgap engineering in graphene and finally rGO features and applications.

Chapter 3 presents the sensor's design process in details, the used viruses, the employed software, and the system's requirements, the chapter sections are: FET design, metal nanoparticles, viruses, COVID-19 spike protein, device testing, electrode-channel interface, and semiempirical model.

Results are presented, compared, illustrated, and discussed in chapter 4. The chapter is sectioned as follows: channel's performance and FET-based biosensor's performance. Finally, chapter 5 states the conclusion and some relevant challenges.

Chapter 2: Literature Review

2.1 COVID-19 Pandemic

SARS-CoV-2 or what's known as "severe acute respiratory syndrome coronavirus 2" was and still the center of extensive research since its outbreak two years ago specifically in early December 2019. The disease was officially first reported in Wuhan City in China, when a group of suspected pneumonia, with unidentified symptoms, cases were disclosed to the World Health Organization, in a matter of days the cases rose up to 282 where four of them were spread across South Korea, Thailand and Japan. Computed Tomography (CT) accompanied with Polymerase Chain Reaction (PCR) tests showed negative results for pneumonia, further tests revealed a genome matching percentages of ~80%, ~50%, ~96% to SARS-CoV, Middle East Respiratory Syndrome Virus (MERS-CoV) and bat coronavirus RaTG13, respectively [1]. Some investigators suspected that the viral infection was originated in a traditional food market in the city since the initial tests of the market surroundings showed corona-virus positive results. As many thoughts that this might be a lab constructed virus the theory was quickly eliminated after confirmation of its animal-origin (bats) backed by the very similar genomic structure of it to the known Coronaviruses i.e., SARS-Cov-1 and MERS-Cov [1-3]. Another compelling evidence was the studies predictions of the imperfection of the binding event between the viral cells and human receptors [4]. Until now seven coronaviruses have been recognized in humans namely, HKU1, HCoV-OC43, HCoV-229E, HCov-NL63, MERS-CoV, SARS-CoV and finally SARS-CoV-2 with the last three being responsible of epidemics [5]. Human to human is the viral transmission method through droplets spread [6], however, in early March 2020 a study has confirmed that SARS-CoV-2 which is originated in bats can be transmitted to humans by pangolin [7] yet more research is still needed to identify other possible hosts. Until the moment no approved therapeutics for SARS-CoV-2 has been found therefore, rapid detection of the virus plays major role in controlling the virus spread and minimizing its consequences.

2.2 Virus Structure

The Corona virus which is a spherical structure with a diameter of 120 nm [8], has a single strand of positive RNA, almost 3000 nucleotides and an arrange of four

structural, 16 nonstructural and five to eight accessory proteins [9]. The random scattering of spikes on its surface revealed a Sun-Corona-like appearance giving it the name of Coronavirus. The virus structure is displayed in Figure 1. Nucleocapsid (N), Membrane (M), Spike (S) and Envelop (E) are the four structural encoded proteins in SARS-CoV-2. With spike protein, which is almost 150 kDa, being the center of many studies because of its vital role in the infection process. It consists of two major subunits S1 and S2. Firstly, S1-subunit attaches to the human receptor enzyme known as Angiotensin Converting Enzyme 2 (ACE2) which are surface structure found on most of the human cells. Then S2-subunit facilitates the human-viral membranes fusion [9-11].
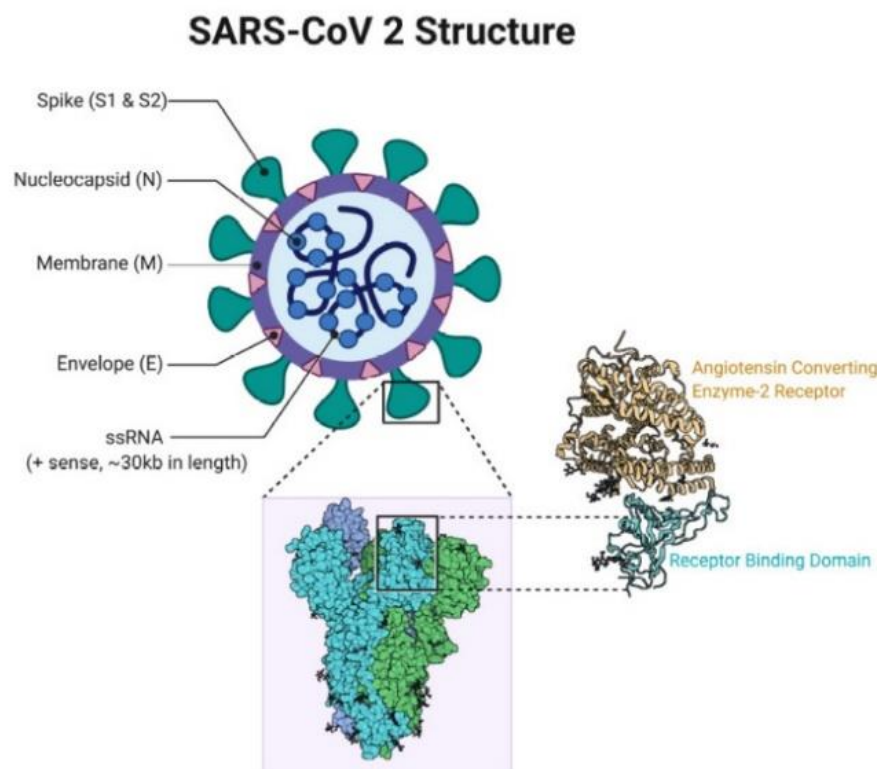
Figure 1: SARS-CoV-2 structure [12]

2.3 Coronavirus Detection Techniques

Since the virus outbreak the medical and research fields have been in a blast to primarily detect and diagnose the virus and then find a vaccine. Different symptoms from fever, cough, breath shortness and fatigue have been detected in SARS-CoV-2 patients, however, these symptoms are not compelling and are very similar to number of other viral infections, hence accurate diagnosing techniques are much needed. Reverse

Transcription Polymerase Chain Reaction (RT-PCR), radiologic photography, chest CT and Artificial Intelligence (AI) were all employed to serve this target, with the molecular approaches having the upper hand since they show more accurate results in targeting specific genomes. According to Udugama's team, the successful production of molecular methods basically depends on understanding firstly, the pathogenic structure and secondly, the alteration in the genes sequences caused by the infection [1]. RT-PCR which is a molecular technique used to target some genes or pathogens in a molecule [13], was firstly used in diagnosis, it can be done either in one or two steps, although the former is faster and can offer reproducible outcomes the latter is more accurate, however, the low sensitivity of this method 60-70% necessitates the use of additional diagnostic tools to support its results [1], [14-15]. On the other hand, chest CTs which play a big role in early detection (especially for questionable RT-PCR results), disease progress monitoring and determining infection severity offered better sensitivity performance compared to chest radiography [16], however, it is still lacking in the early stages of infection owing to its inability to detect Ground-Glass Opacity (GGO) [17-19]. Moreover, since the CT results are not evident, many medical societies have advised to not use it as a diagnostic tool owing to the increased infection-spread risks that may unfold when moving the suspected patients around the hospital for a CT scan [20-21]. In a trial to overcome the mentioned shortages, a collaboration between different affiliations in China and Netherlands conducted a study to correlate the chest CT with the RT-PCR results on 1014 patients the outcome of the study was, chest CT sensitivity for detecting COVID-19 were better compared to RT-PCR nevertheless, many studies recommend using both approaches to increase the detection accuracy and support the results [15], [22]. As the infected numbers surged noticeably, the manual classification of the RT-PCR tests and CT scans results became a tedious and time consuming task, the use of more efficient, accurate and rapid approach was a necessity hence Artificial Intelligence (AI) was employed to help tackle this pandemic. Artificial intelligence was used in several occasions such as forecasting virus spread, contact tracking, SARS-CoV-2 cases monitoring, and early diagnosis to help the medical staff [23]. AI accompanied with radiological photography was proposed, a binary (with positive, no findings classes) and multiclass (with positive, no findings, Pneumonia categories) classification with

accuracies of 98.08% and 87.02%, respectively, was achieved by Tulin Ozturk's team [24]. In [25], Hemdan's group with the use of seven convolutional neural network models developed deep learning network using 50 radiographic images with 25 of them are confirmed COVID-19 cases. Detection of GGO in X-rays using deep learning network called nCOVnet was introduced, the possibility of data leakage in this network was eliminated during training so the results were unbiased, the overall accuracy reached up to 88.1% [26]. Another promising diagnosing technique named as "Reverse Transcription Loop-Mediated Isothermal Amplification" RT-LAMP was introduced by Zhu's team [27], the newly emerging technique showed a superior specificity compared to RT-PCR (assay's specificity and SARS-CoV-2 analytical sensitivity is 100%), a collection of primer sets, opening reading frame and SARS-CoV-2 N genes were amplified in a single tube reaction to finally be diagnosed by a lateral flow biosensor, the whole diagnostic process takes up to 1 hr, however the number of samples in the study was small and the method was not evaluated for other types of clinical samples. Clustered Regularly Interspaced Short Palindromic Repeats (CRISPR-Cas), a pending-clinical-validation technique that was previously used to detect bacteria, microRNAs, and cancer mutations, has been tried for SARS-CoV-2 diagnosing. With a time span less than 40 minutes, 95% positive predictive agreement, 100% negative predictive agreement, and clinical samples validated results the approach provides a good, accurate and rapid alternative to RT-PCR [28]. Summary of techniques and their merits & demerits is found in Table 1.

Table 1: Summary of COVID-19 detection techniques

Ref.	Used Technique	Advantages	Disadvantages
[1], [14-15]	RT-PCR	One step: rapid and reproducible results Two steps: better accuracy	One step: lower accuracy Two steps: time consuming Both: expensive kits
[17-19]	Chest CT	High sensibility, availability of tools	Low sensibility in early stages
[23-26]	AI accompanied with RT-PCR and chest CT	Rapid, simple, reduce the number of needed radiologists, save time	still didn't reach 100% classification accuracy
[27]	RT-LAMP	High specificity, rapid (1 hr)	Tested on few samples and wasn't evaluated for different clinical samples
[28]	CRISPR-Cas	Rapid (less than 40 mins)	Pending clinical validation

2.4 Biosensors for Viral Detection

The battle between human and viruses has always been ongoing, several different viruses such as Marburg, Ebola, HIV, Smallpox, and many others have threatened the human race throughout the decades. Researchers have used different diagnostic techniques to eliminate and minimize the effect of such outbreaks. One of the most commonly used devices are electromechanical biosensors. Reduced accuracy, sample treatment, time consuming, the need for experienced staff and higher costs are all shortages introduced by conventional methods such as Lateral Flow Assay and ELISA that can be overcome by using such sensors [29]. Electromechanical biosensors fall mainly into four categories namely: nucleic acid-based, antibody-based, aptamer-based, and antigen-based. Sensors basically consists of receptors and transducer, when a specific target (protein, nucleic-acid or antibody) is detected by the receptor a reaction occurs resulting in a signal that can be processed by the transducer [30]. Basically, a DNA-based biosensor recognizes a complementary DNA sequence by hybridization due to a single stranded restrained probe on its transducer surface. Its low cost, suitability for large-scale fabrication, and rapid response attracted a lot of attention to it [31]. In [32] a DNA based biosensor was introduced to detect the Ebola virus where the biosensor has remarkable sensitivity due to the enzyme-amplified recognition used in it. The sensor has gold electrodes and employs a sole DNA strand as the probe. DNA hybridization was again introduced by Manzano M. et.al but this time the target was hepatitis A virus. The label free FET was tested against different viral and bacterial specimens using nested RT-PCR technique. It achieved a Limit Of Detection (LOD) of 6.4 fg/µl [33]. Antibody-based or immunosensor which is another type of electrochemical biosensors depends on the binding event between antibody and antigen which results in a signal that can be sensed by the transducer however its stability and reproducibility still needs enhancing [34-35]. Ebola virus was also the center of Chen et al. work [36], where a reduced Graphene Oxide (rGO) based Field Effect Transistor (FET) was designed to detect the Ebola antigen. The rGO sheet was sprayed with gold nanoparticles for antibodies anchoring, and the limit of detection reached up to 1 ng/ml. Anik et al. [37] detected influenza A virus. The designed sensor utilized composite graphene-Au electrode to measure the neuraminidase activity with LOD of 10-8 U/ml [37]. Aptamers, the product of

Systematic Evolution of Ligands by Exponential Enrichment (SELEX) method, are oligonucleotides that are short and single-stranded. Their most appealing feature is the noticeable affinity and sensibility against targets which makes them excellent to use in biosensors [38-39]. In [40], Lum et al. targeted Avian Influenza (AIV H5N1) virus. They designed an impedance aptasensor with a detection time of 30 minutes. The electrodes were coated with gold and then altered with streptavidin. The binding event of the virus causes an impedance increase which is proportional to the virus concentration [40]. H1N1 virus which is the cause of influenza A was targeted in this paper [41]. An EIS aptamer-based sensor was introduced. The sensor with gold electrodes showed high affinity toward H1N1 virus. The sensor was also tested against influenza B and parainfluenza viruses. Moving on to the final type of biosensors namely antigen immunosensor. These particular sensors have antigen-treated electrodes to detect flowing antibodies [30]. Enzyme-linked immunosorbent assay or what's known as ELISA was, for recent years, the golden technique when targeting viral antibodies, however this technique suffers from several disadvantages such as the need for big, expensive, fully equipped laboratories as well as trained staff to run the process. Moreover, its sensitivity and antibody's stability are questionable [42-43]. Capacitive highly sensitive biosensor for the detection of Zika Virus (ZIKV) was the product of this research. The mentioned sensor consists of ZIKV's antigen-treated nanowire which can detect up to 10 antibodies in 30 μL specimen. Different antibodies were employed to validate the sensor's performance. The experiments showed a change in the capacitance against the target, while no noticeable change was observed against other antibodies. This change was confirmed to be proportional to the target's concentration [44]. Hantavirus was targeted in [45], where Jeferson's team created a gold surface modified with the virus protein via self-assembled monolayer formation which can insure the presence of target's antibodies in human serum. Coupling of the mentioned protein was achieved by immersing the electrodes in an antigen suspension. Good sensibility against the virus antibodies was reached [45]. Table 2 compares the different categories of biosensors and their uses.

Table 2: Biosensors categories

Ref.	Sensor's Category	Detected Virus	Advantages
[32]	Nucleic-based	Ebola	Rapid response, cost friendly, suitable for large-scale production
[33]		Hepatitis A	
[36]	Antibody-based	Ebola	High affinity, high sensitivity.
[37]		Influenza A	
[40]	Aptamer-based	Avian Influenza	Low cost, low toxicity, reproducibility, easy & quick to fabricate, high sensitivity, stability
[41]		Influenza A	
[44]	Antigen-base	Zika	High affinity, high sensitivity
[45]		Hanta	

2.5 Biosensors for SARS-CoV-2 Detection

As the virus spread is still exacerbating, efforts continue to be channeled into finding the best path to control the recent global situation. Medical authorities are making huge efforts in supporting any potential detection-tools, therapeutics, and vaccines productions. Basically, three vital factors are not to be tolerated when detecting SARS-CoV-2 namely identification targets, detection methods, and measured signal's amplification and transducing [46]. The viral infection can be spotted by detecting one of the following: complete virus, viral RNA/DNA, and antibody/antigen [9]. In 1986 Gerd Binnig and Heinrich Rohrer were able to introduce a major nanoscience technology known as "scanning probe microscopy" which made it possible to perform experiments and studies on the nano-scale level [47], on such tiny scales most of known physics become invalid that's where nano-science comes in. As the electrodes' size reduction continues to happen, the common behaviors and properties becomes harder to predict. The electrodes at the nano range can be treated as 1D devices owing to the electrons' travel distance between two scattering events being greater than the atomic size and as a result the resistivity and hence the conductivity becomes independent of the electrodes' length [48], this has to be taken into consideration when designing any Field Effect Transistor's (FET) electrodes. FET with the help of 2D semiconducting materials were utilized to detect SARS-CoV-2, depending on the easily altered electronic nature of such materials and their sensitivity. It can offer a rapid detection solution. The group used SARS-CoV-2-antibody functionalized semiconducting Transition Metal Dichalcogenide (TMDC) WSe2 monolayers as the detection platform and reached a LOD of 25 fg/μL in 0.01X Phosphate-Buffered Saline (PBS) [49]. Graphene based FETs was also employed

to detect the virus. After preparation of the graphene layer Au/Cr electrodes were etched using thermal evaporation and lift-off methods. Then, the graphene channel was coated with antibodies against the viral spike protein. The sensor's performance was tested and validated and it reached a LOD's of 1.6 x 101 pfu//mL and 2.42 x 102 copies/mL in culture medium and clinical samples respectively [50]. Nanomaterials based sensors and assays also played a major role in the detection race. Huang et al. designed a AuNPs decorated lateral flow strips to detect the produced IgM antibodies against SARS-CoV-2 [51]. A configuration of an anti-human IgM-AuNP was the sensing probe. Blood serum from infected and healthy controls were utilized to test the assay's suitability which reached a 100% and 93.3% sensitivity and specificity, respectively. Again, AuNPs were employed in this research with SARS-CoV-2 spike protein antigen (SARS-CoV-2 Ag) being the detection target. Mahari's group [50] designed a AuNPs decorated, fluorine doped and nCovid-19 monoclonal antibody (SARS-CoV-2 Ab) coated tin oxide electrode (FTO) as a potentiostat sensor to sense any change in electrical conductivity, and then compared its performance with an in-house built eCovSens potentiostat. Both sensors displayed high sensitivity in early stages of detection. LOD's of 90 fM and 120 fM for eCovSens and potentiostat, respectively, were recorded [52]. The applicability of another interesting nanomaterial named Quantum Dots (QDs) was evaluated for SARS-CoV-2 diagnosing. Quantum Dots (QDs) which are nanometer sized semiconductor particles with attractive properties [53] are very promising candidates that yet to be utilized in the diagnosing and detection of SARS-CoV-2 field according to Sultan et al.'s review [54]. Plasmonic Photothermal (PPT) effect along with Localized Surface Plasmon Resonance (LSPR) was suggested. The production of PPT heat on the complementary DNA functionalized, nano-sized gold islands give rise to the in-situ hybridization temperature and leads the specific differentiation between couple of similar genetic sequences. This technique is very sensitive, rapid and reach a LOD of 0.22 pM [55]. Surface-Enhanced Raman Scattering (SERS) concept was recently employed. Zhang et al. proposed a SERS based biosensor to detect SARS-CoV-2 in untreated saliva. The sensitivity and reproducibility were guaranteed by using three-phase (oil/water/oil) liquid-liquid system which make up two layers of AuNPs. The interaction between the viral spike antibody, spike antigen protein and Raman silver

nanoparticles was the focus of the sensing event. with no need for any sample preparations the sensor can sense infection at concentrations of 6.07 fg mL-1 in untreated saliva [56]. Technologies used in SARS-CoV-2 detection are depicted in Figure 2.
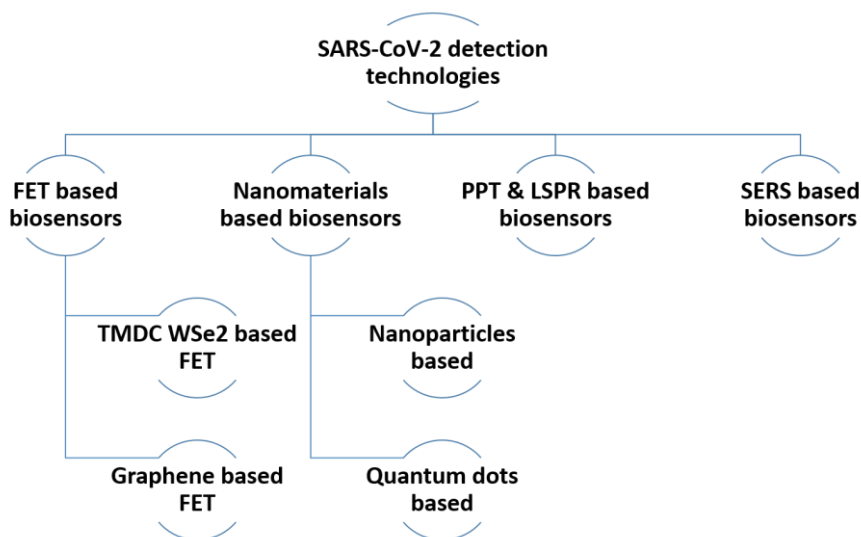
Figure 2: SARS-CoV-2 detection technologies

2.6 Graphene

Carbon which is the primary material of all living structures can be found in different arrangements around us, for example it can be spherical forming fullerenes, or rolled along specific direction giving carbon nanotubes. It can also be in a three-dimensional structure producing weakly bonded graphene layers known as graphite and it may be found in a honeycomb-like arrangement revealing graphene [57]. Graphene which was firstly discovered in 2004 [58] is a single layered, 2D with hexagonal lattice structure material. Since its discovery, graphene has become the center of numerous research work because of its attracting electrical, mechanical and optical properties. Owing to its perfection as a 2D material it has earned the description of "ultimate flatland" [59]. Basically, the honeycomb lattice comprises of two inter-bonded sublattices A and B as depicted in Figure 3. Therefore, a single unit cell has two carbon atoms. Each carbon atom in the lattice has a total of four bonds (one s and three p orbitals). Three are σ (one s and two p orbitals) which don't have any contribution to the graphene conductivity since they are well covalently bonded to the graphene hexagonal lattice, and one is a

perpendicular z-directed π bond (one p orbital) which then all π bonds together forms what's known as the π (valence) and π* (conduction) bands, with these bands being responsible for most of the unique graphene electronic properties [57], [59-61]. From a band structure point-of-view graphene is a gapless semiconductor since its conduction and valence bands are touching as displayed in Figure 4. These touching points are called Dirac points (K & K'). Unlike most of semiconductors which focus on the zero-momentum point Γ when studying electronic properties, K and K' points are the focus for graphene. This is not the only difference between graphene and conventional semiconductors, there are a number of interesting differences to be mentioned. Firstly, energy band gap, graphene is gapless while other semiconductors have finite gaps. Secondly, graphene has a chiral, linear dispersion relation, however semiconductors have quadratic one. Thirdly graphene is much thinner compared to 2D electron gas, in fact it is the thinnest material found until now. Finally, graphene has finite minimum conductivity, irrespective of diminishing fermi energy, which is a key point to be noted when designing FETs [60]. To further understand the graphene's electronic behavior, Geim and MacDonald [59] have employed massless, relativistic particles as a reference since both graphene and mentioned particles own a similar Hamiltonians. Klein paradox for these particles implies that the transformation of them into virtual antiparticles leads to the penetration of any-size potential barrier. This paradox has never been witnessed in particle physics until graphene which explain its extraordinary conductivity. This fascinating phenomenon could be understood by comprehending the Hamiltonian, which for graphene allows simultaneously the positive and negative energy states leading to a perfect transmission (no reflection) for infinite barrier [62]. When comparing the particles' interactions in graphene to those of fermions in Quantum Electrodynamics (QED) one can find that graphene ones are noticeably stronger owing to the weaker mutual screening of electrons and the lower coupling constant [59], [61].
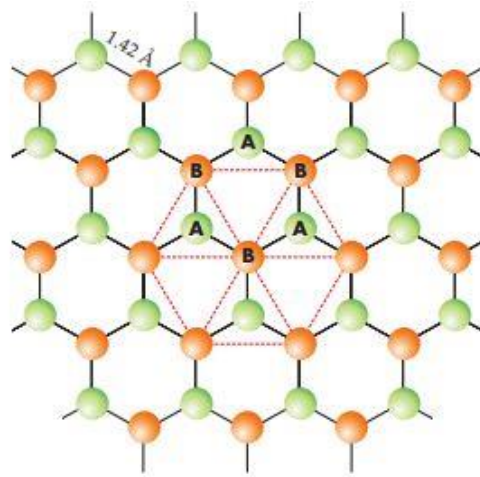
Figure 3: The graphene honeycomb lattice [59]
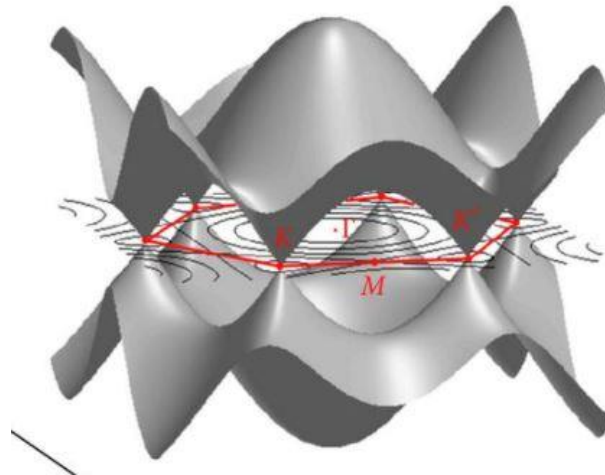
Figure 4: Graphene band structure [60]

2.7 Bandgap Engineering in Graphene

Graphene with its extraordinary features may be at its raw state not suitable for electronics applications. The gapless nature of graphene prevents it from being used as a channel material in FETs. The presence of two identical carbon atoms within the unit cell causes the absence of any energy gap. Thus, to open a bandgap the planar symmetry should be broken by structural or chemical modifications [63]. The first attempt to engineer a bandgap in a semiconducting material with the intention to tailor a device properties is dated back to 1957 by Professor Herbert Kroemer [64]. According to Frank, until 2010 three ways had been investigated to open a bandgap in graphene. The first one

is by introducing graphene nanoribbons [65]. The size constraints that are applied on them apparently open a bandgap that is inversely proportional to their width. However, fabrication imperfections limit this approach from being commercially adopted. Secondly, applying a vertical electrical field on bilayer graphene opens a bandgap that can reach up to 200-250 meV with increasing displacement electrical fields [66-67]. And thirdly, simulations have proved that strain can be a mean of bandgap engineering in graphene [68] nevertheless, the applicability of this method is still under question. In 2011, an approach combining two of the above mentioned methods were designed [69], where uniaxial strain was applied on graphene nanoribbons. The study revealed that the energy gap was more affected by compression than tensile deformation. Vagdevi's team noticed that instead of applying a high electrical fields to Bilayer Graphene (BLG), the use of single-side metal adsorption leads to breaking the bond symmetry which eventually opens a bandgap in graphene. $SnCl_4$ metal was physisorped by BLG causing a band gap opening and a shift in fermi level [70]. Graphene's fermi level is sensitive to any contact, which paved the way for fermi level tuning that causes a change in charge carrier concentrations. The process of altering graphene's lattice structure by replacing or adding atoms is known as doping which is a mean of tailoring graphene's electronic structure. As reported by Lee et al. doping can be introduced by two methods 1) carbon atoms exchange with heteroatoms 2) the addition of chemically or physically surface adsorbed atoms [71]. The two approaches and the alternating electrical chemical environment were investigated in a density functional theory study which showed that, although a bandgap opening is achievable by surface bonding, it negatively affects the linear dispersion relation of the band structure. Moreover, isoelectronic co-doping and the alternating environment didn't offer a much superior behavior in terms of mobility and compared to conventional semiconductors [72]. The literature has many examples of elements that have been used as adsorbents to tailor graphene electronic properties namely, phosphorous [73], chromium [74], oxygen and nitrogen [75], and boron [76]. Even water molecules were added as dopants to graphene [77]. The addition and removal of oxygen by oxidation and reduction also played a major role in this regard. Oxidation of graphene leads to the introduction of its oxide "Graphene Oxide" (GO) and then the reduction of it produces "reduced Graphene Oxide" (rGO). Studies and

observations on these materials prove that the latter is a perfect candidate to be used as a FET channel material since the introduction of oxygen functional groups opens a bandgap in graphene therefore a tuning of electrical and structural properties including bandgap can be achieved by controlling the level of reduction [78-80]. In [80], the effect of a single and many functional groups in addition to other possible formed structures have been studied. The study revealed that epoxy and hydroxyl groups prefer to aggregate together. The addition of a single functional group can induce some bound states which may lead to altered transport properties and open significant band gaps that can be tuned with controlled oxidation process. Yiqian's team has also performed an experimental study on graphene's bandgap tuning by the addition of nitric acid HNO_3 during the oxidation process. Their experiment showed that with an increasing concentration of HNO_3, the surface epoxides linearly increased without introducing any inter-planar defects causing the bandgap to change from 0.264 to 0.786 eV [79]. The relationship between the epoxies and hydroxyls and bandgap tuning was also confirmed in earlier work [81-82]. Figure 5 summarizes the bandgap engineering methods in graphene.
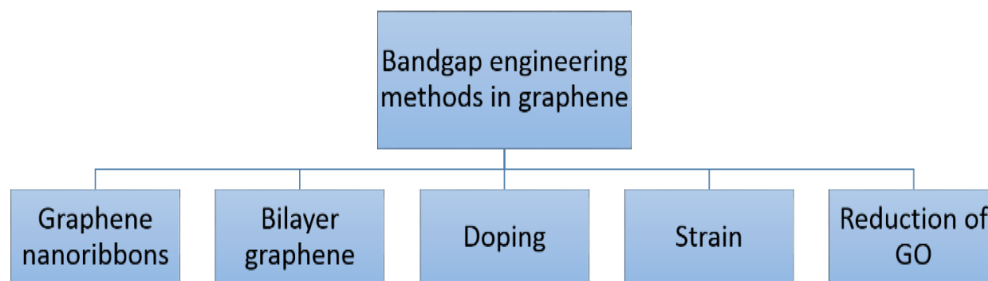
Figure 5: Bandgap engineering methods in graphene

2.8 RGO Features and Applications

Reduced Graphene Oxide (rGO) as a derivative of graphene enjoys several unique electrical properties. The existing functional groups on its surface pave the way for increased control and tuning of its electronic behavior. For example, it was proved that the reduction of GO in hydroiodic acid, the productivity undergoes a noticeable improvement with a resistivity reduction factor of 103 reaching a minimum value of 0.003 Ω.cm [83]. Hydroiodic acid was again used by Wei and Giorgio to tune the rGO's

oxygen content from concentrations of 0.06 to 0.95 mol L-1 resulting in electronic properties tailoring [84]. Moreover, as mentioned previously controlling the degree of reduction is also a mean of bandgap tuning [78-82]. Literature has also investigated the dependence of transparency and conductivity on the GO degree of reduction and its films' thickness [85]. The degree of oxygen functional groups elimination was again the reason of decreasing the rGO interlayers spacing's which eventually means altered electronic features [86]. In addition to the aforementioned benefits offered by oxygen functional groups, they are also considered as active binding sites for the desired molecules such as nanoparticles or antibodies which allow further engineering of rGO sheets [84-85]. Figure 6 illustrates the advantages offered by controlling the amount of oxygen functional groups in rGO. RGO has been extensively utilized in several FETs biosensors. In the work done by Yu et al. [88] two micropatterned solution gated rGO FETs were designed to detect nucleoside triphosphates. Both sensors showed similar ambipolar field effect behavior. Their investigation reached the conclusion of the modification of the FET by bis-pyrenyl derivative can enhance its sensitivity to reach a LOD of 400 nM. Solution gated rGO FET was also used for pH sensing where a series of enzymatic reactions produce protons ($H+$) that can be detected by the rGO channel which was decorated with a nerve-system's neurotransmitter [89]. Additionally, proteins [88-89]. Viruses [36], [90-91], gases [94], PNA-DNA hybridization [95] and bacteria [96] have all been discriminated and detected by rGO FET based sensors.
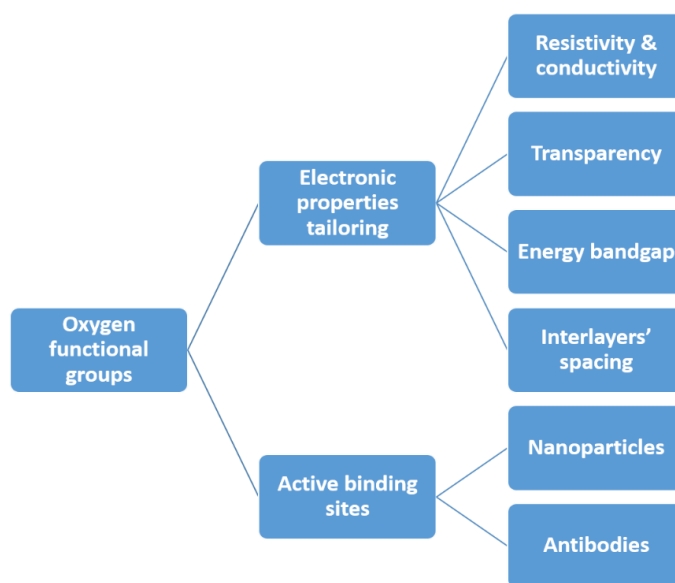

Figure 6: Oxygen functional groups roles in rGO

Chapter 3: Semi-Empirical Modelling and Simulation Settings

3.1 Introduction

In this chapter a simulation-based research on the molecular scale is conducted using Quantumwise (ATK-VNL) package [97]. The study focuses on the FET-based sensor's electronic transport properties including transmission spectrum, conductance, and electrical current. The sensor's performance was investigated by utilizing a semi-empirical approach along with non-equilibrium Green's function.

3.2 FET Design

According to Clemens et al. study Field Effect-Based Biosensors (BioFETs) suffer from two major challenges. First, getting an accurate accepted results is based on the self-consistent calculations that must include all the charges of the system. Second, BioFETs arrangements have multi-scale nature i.e., the biomolecules are on the Angstrom scale while the device can reach to micrometer range [98]. It was indeed a big challenge for this research to overcome these challenges since the used software had to deal with a large system (>6000 atom). FET basically consists of two electrodes, semiconducting channel, and a gate where the whole arrangement is placed on a dielectric layer (in this case Silicon wafer covered with SiO_2 dielectric) to prevent any unwanted electrical interactions. The gate is connected to an external circuit to control its voltage which is eventually used to alter the conductance of the channel. When the FET is operational a bias is applied between its electrodes, known as the drain and source, the bias can be in the range of 2-3 V. To comprehensively describe a FET performance several metrics are of interest such as channel's conductance, current, transconductance (ability to translate the smallest voltage change into a noticeable current change), and Dirac point or Charge Neutrality Point voltage (CNP) behavior [99]. The rGO-FET based biosensor performance was investigated by generating gate voltage (V_g) versus drain-source current (I_{ds}) curve and drain-source voltage (V_{ds}) versus drain-source current (I_{ds}) curve. The upcoming sections illustrate our FET design process using the Quantumwise ATK software.

3.2.1 Electrodes

Following the literature mentioned previously that electrodes at nano-size can be treated as 1D object [47-48], here in our design we have kept in mind the size requirements (being as small as possible) with the intention of speeding up the simulation process. The electrodes' size's compatibility was further confirmed from the convergence of the software simulations, moreover the selected dimensions showed the optimum behavior. The simulated electrodes are golden, with a length and width of 11.89 Å and 60.56 Å (1.189 nm, 6.056 nm) respectively as shown in Figure 7. Dirichlet condition along C direction and Neumann boundary condition along A and B directions were applied on the electrodes when studying the device's performance.
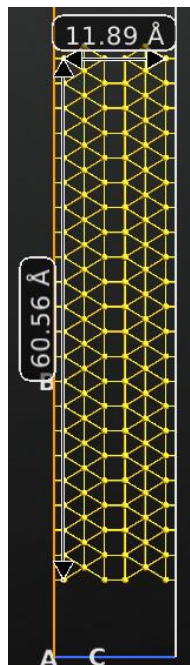
Figure 7: Electrodes dimensions and geometry

3.2.2 Channel

When designing our reduced Graphene Oxide (rGO) channel the below points were followed:

- Graphene nanoribbons falls into two main categories depending on their edges shape namely, zigzag and armchair as shown in Figure 8. The former one has metallic nature and hence can't be used as a channel material while the latter can be either metallic or semiconducting based on the width, however since the

channel here is narrower than 10 nm it can be considered as semiconductor [100-101]. This conclusion was further investigated by Quantumwise ATK software and the results are discussed in the coming sections.

- Oxygen functional groups spread on the surface of rGO randomly, actually this is one of the challenges when dealing with graphene, each sample has its unique structure therefore, it is difficult to produce identical samples with the exact same electronic behavior [102]. Studies have found four types of oxygen containing groups in graphene namely, hydroxyl (C-OH), epoxide (C-O-C), carboxyl (COOH), and carbonyl (C=O) with the former two being located at the basal plane and are responsible for most of the graphene's unique electronic properties while the latter ones were found on the edges [103-107]. The channel designed here contains only hydroxyl and epoxide groups since carbonyl are not stable and converts into epoxide whereas carboxyl is only stable on defects sites which is not presented in our channel [79].

- Channel dimensions were mainly selected based on the viral spike protein size the channel is 6.124 nm long, 5.896 nm wide as illustrated in Figure 9 below. It is expected that the energy band gap would get significantly smaller or even diminishes if the channel's width is further increased according to Poljak's study [108]. Moreover, it is anticipated that any further increase in the channel's width will also reduce the transmission which will definitely result in a current reduction this is attributed to the increased contact resistance caused by the channel's width increment [108]. However, similar trend in terms of transmission and drain current variation is foreseen for changed size, these variations are caused by the binding event between the antibodies and the spike protein. While no detectable change in transmission and current will appear in case of other viruses since no binding event is expected.

- Channel functionalization basically constitute of three main components namely, MNPs, bio-recognition molecules and edges passivated with hydrogen.

- MNPs are employed here for two major reasons. First, since the surface of graphene is not chemically suitable for direct immobilization of biomolecules, Metal Nanoparticles (MNPs) are often used on rGO to enhance its bio-sensing

performance and specificity. Biocompatibility, surface-biomolecules immobilization and selectivity were all proved to be enhanced when employing MNPs [109-111].

- Secondly, another reason for using MNPs is to avoid the immediate interaction between the rGO channel and the biomolecules, this is so important since the antibodies' immobilization can impact the electronic structure of the rGO such as conductance and electrons distribution [112]. It is worth mentioning that the electrons' alteration generated by such immediate interaction is undesirable since it introduces Negative Differential Resistance (NDR) behavior which was proved in our study and will be discussed in later sections

- Bio-recognition molecules are used to further enhance the selectivity of the sensor and amplify its affinity. The rGO channel was coated with COVID-19 antibodies which are specific against the viral spike protein and known as probes. The antigen-antibody binding event is responsible for the channel's altered electrical properties and considered as detection evidence [91], [113].

- The rGO channel edges were passivated with hydrogen. This step is crucial to saturate the dangling bonds, increase the edge-carbon stability, and effectively open a bandgap [114-115].
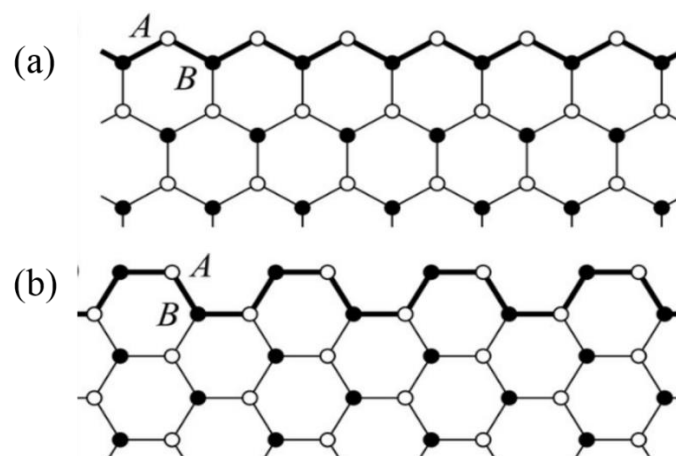

Figure 8: Nanoribbons structures a) Zigzag nanoribbon b) armchair nanoribbon [116]
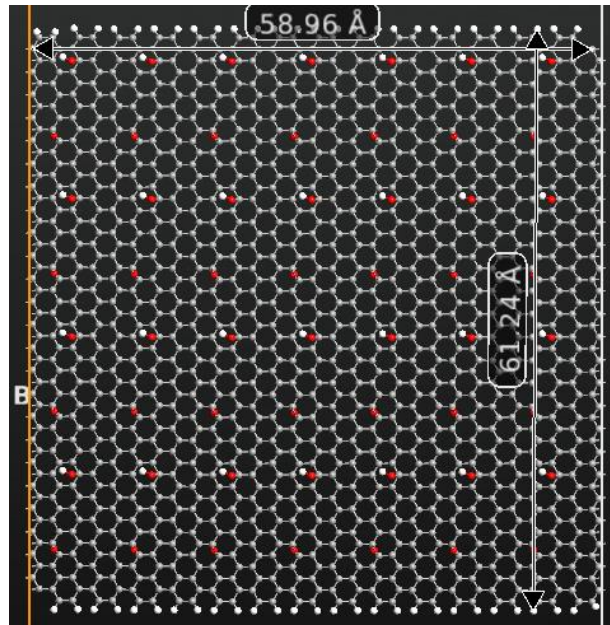
Figure 9: Designed rGO channel (Color code: oxygen-red, hydrogen-white, and carbon-grey)

3.2.3 Gate

According to literature the gate electrode can be placed either on top, back or top and back (dual structure) of the channel. Top gate structure is useful for high frequency applications since it provides a precise control of the graphene channel, on the other hand back gate installation is more suitable for bio-sensing and photo-detection applications because it allows the graphene channel to be in full contact with the detection medium. Another structure which is a combination of the above mentioned structures is the dual gated. Dirac point control can be achieved by the dual gate structure which has a wide range of applications [117-118]. When the rGO channel is exposed to the detection medium, its properties are altered. This alteration in the channel's charge carriers' is measured as the density and conductivity. The gate for the designed sensor is placed at the back of the channel but not touching it. The gate thickness is 1Å and it consists of two layers: a dielectric layer of silicon dioxide with a relative dielectric K = 3.9 and a metallic layer. Top and side views of the full FET device is shown in Figure 10.
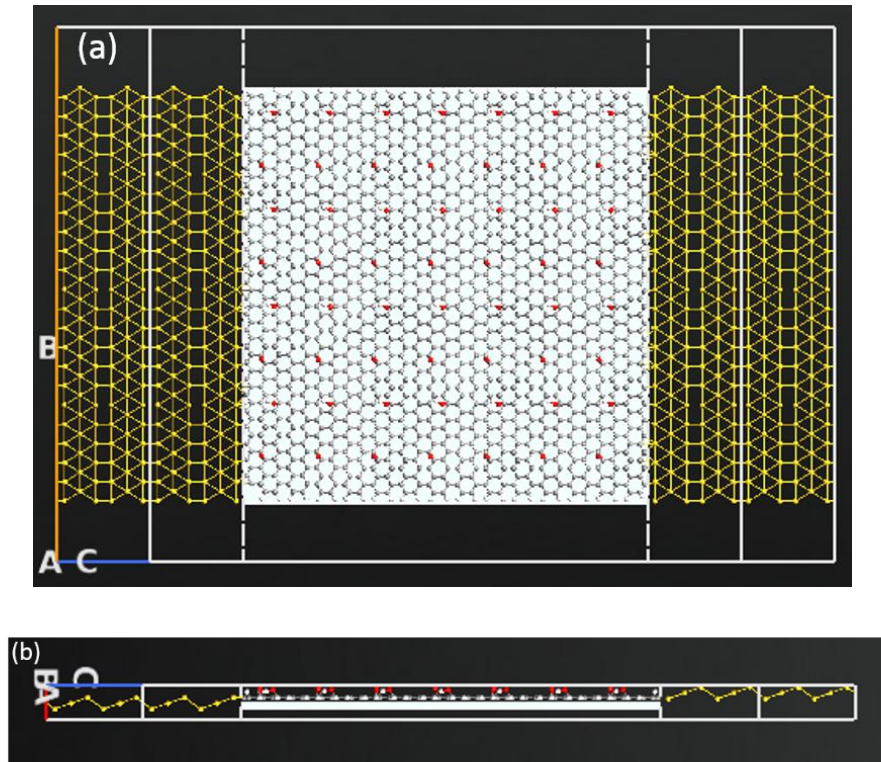
Figure 10: Full FET device a) top view b) side view

3.3 Metal Nanoparticles

As mentioned previously in the literature review chapter, oxygen functional groups act as binding sites for nanoparticles, coming from this all MNPs here will be placed on hydroxyls or epoxies [87]. Graphene/MNPs structures are very interesting, the outstanding conductivity of graphene along with the MNPs noticeable reactivity paves the way for several applications such as, controlling the spatial localization of the surface plasmon resonance of the metal particles, graphene surface's light absorption boosting, catalytic activity enhancement and the addition of bio recognition molecules [109]. Within the scope of this study different MNPs will be added on the sensor's rGO channel namely, copper and silver, the sensor's performance, bare and MNPs decorated, in terms of electrical current and selectivity will be compared and investigated. A special plug-in builder known as Wulff Constructor in the Quantumatk software was used to build the MNP's, the builder provides two building options whether to provide the nanoparticles' radii and cut-planes' surface energies or ready structures can be inserted from the database. The radii of the added MNPs is 5Å, figure 11 below shows the used nanoparticles structures.
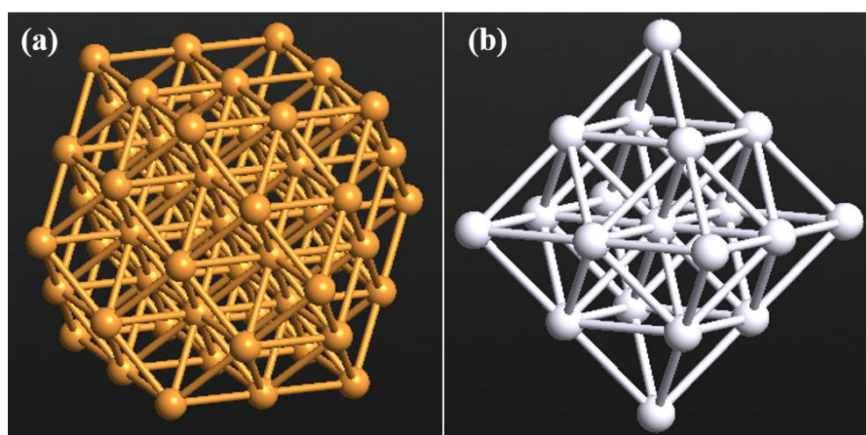
Figure 11: The added MNPs with 5Å radii a) copper b) silver

3.4 Viruses

3.4.1 COVID-19 Spike Protein

As stated earlier, COVID-19 spike protein is the target to be detected by the designed sensor. In this research the spike protein was imported from an online protein data bank named RCSB Protein Data Bank [118, 119]. The PDB ID of (Spike protein) is 2IEQ [121], while the PDB ID of (COVID-19 virus spike receptor- binding domain complexed with a neutralizing antibody) is 7BZ5 [122]. Additionally, Rabies virus was also imported to test the sensor selectivity, the virus's PDB ID is 7C20 [122]. The COVID-19 spike protein is shown in Figure 12. It is evident from the figure that the spike protein has a large size (~5000 atom) which was a big challenge for this study in terms of simulation time, and available computing nodes. Moreover, the spike protein was placed on the MNP's as discussed earlier. Figure 13 shows the biosensor conjugated with MNPs, bio molecules, and spike protein.

3.4.2 Device Testing

Another virus was tested via Quantumwise ATK software. This step is essential to test the biosensor's selectivity. The sensor is expected to show no significant change in the transmission spectrum when exposed to the other viruse, since the employed sensing probes are SARS-CoV-2 antibodies. The virus used here is the Rabies [124] which is shown in Figure 12b. It was chosen based on its small size (~1000 atom) to reduce the computational load and time. The sensor was coated with bio molecules as sensing

probes, in this case anti SARS-CoV-2 human neutralizing antibody was employed [125] as shown in Figure 12c. Figure 14 demonstrates the structure with the antibody, MNPs and Rabies virus.
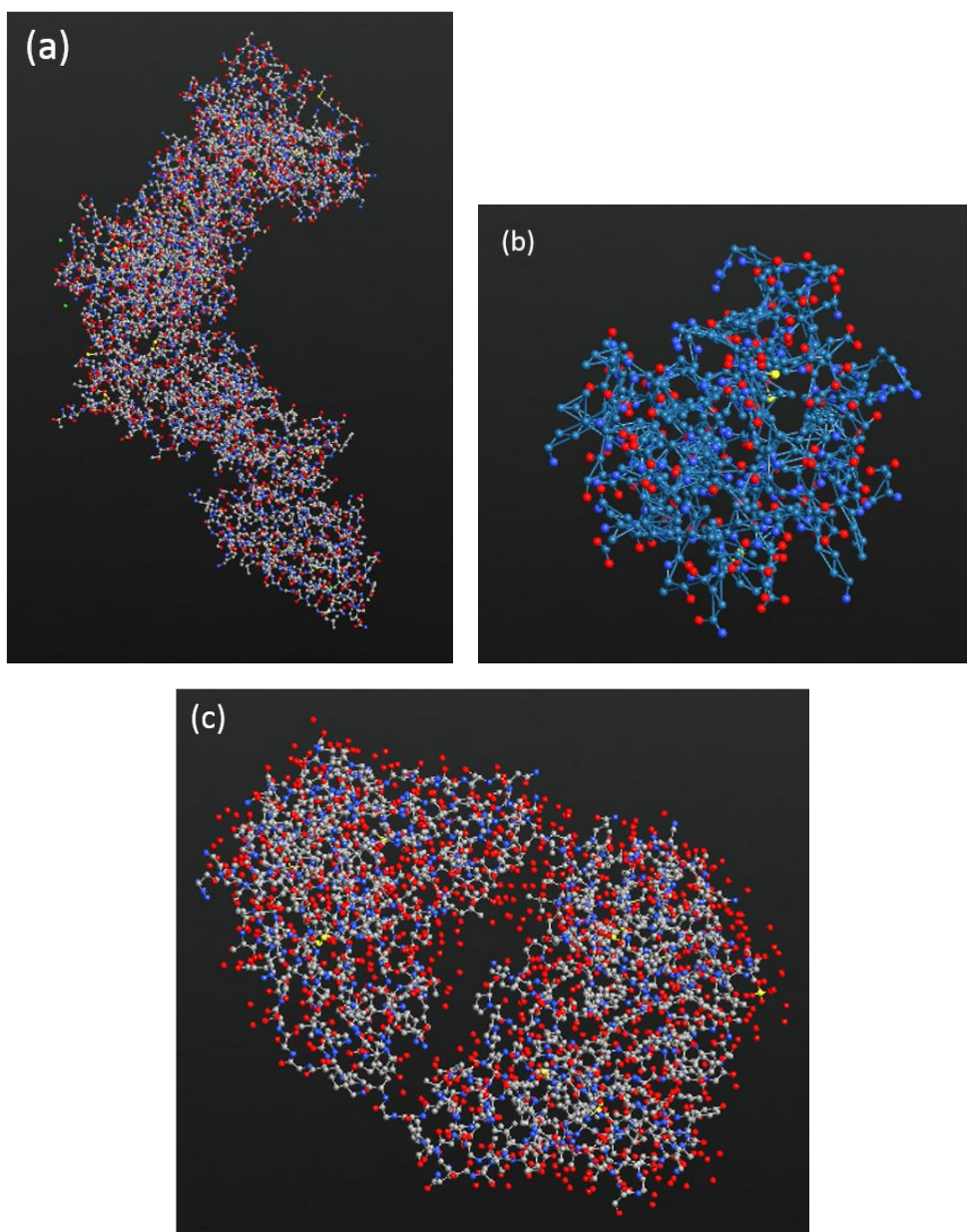
Figure 12: Different structures imported into the Quantumatk software a) the imported viral spike protein b) Rabies virus c) anti SARS-CoV-2 human neutralizing antibody
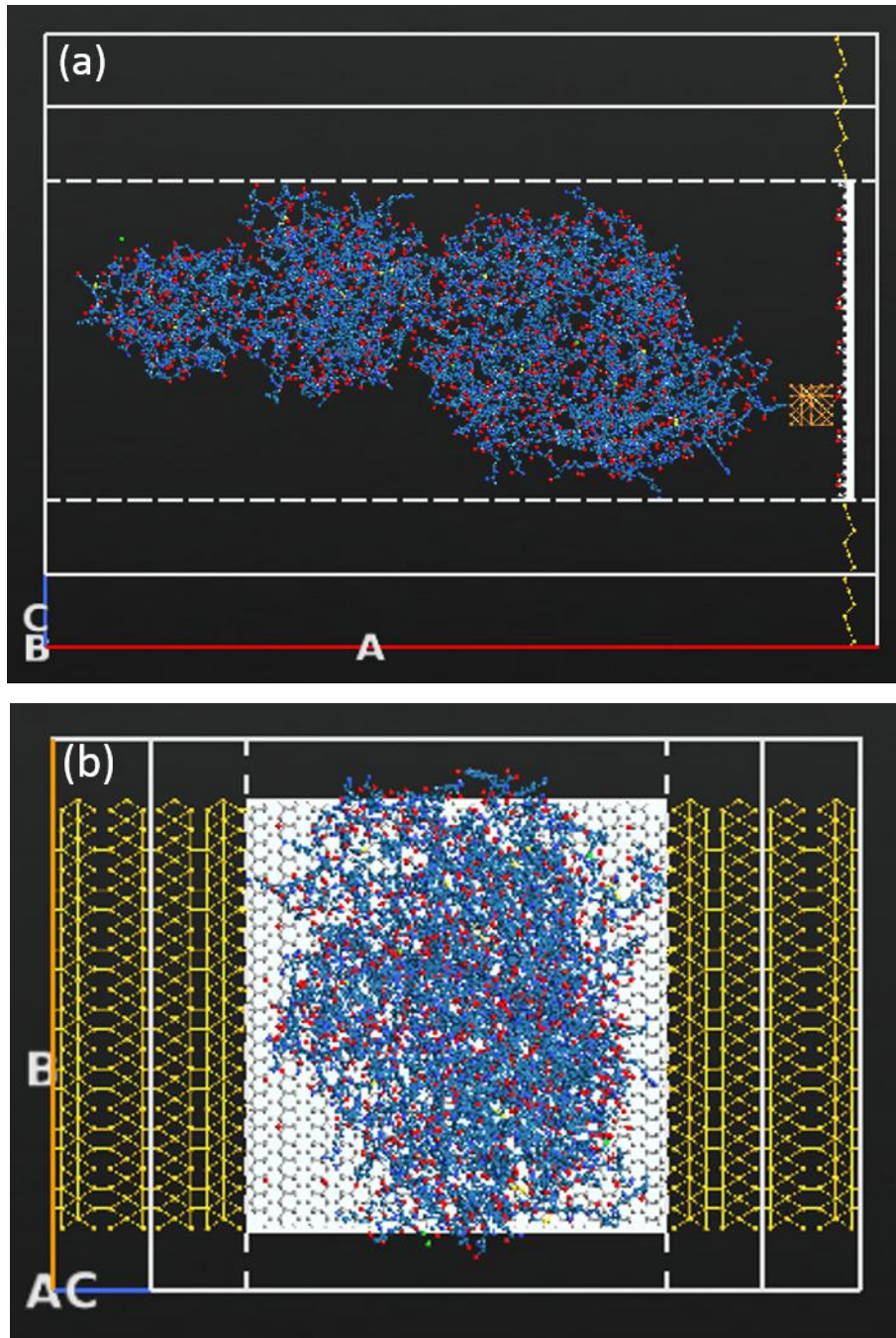
Figure 13: Different views of the sensor a) side and b) top views of the sensor with Cu MNPs, COVID-19 antibody and COVID-19 spike protein
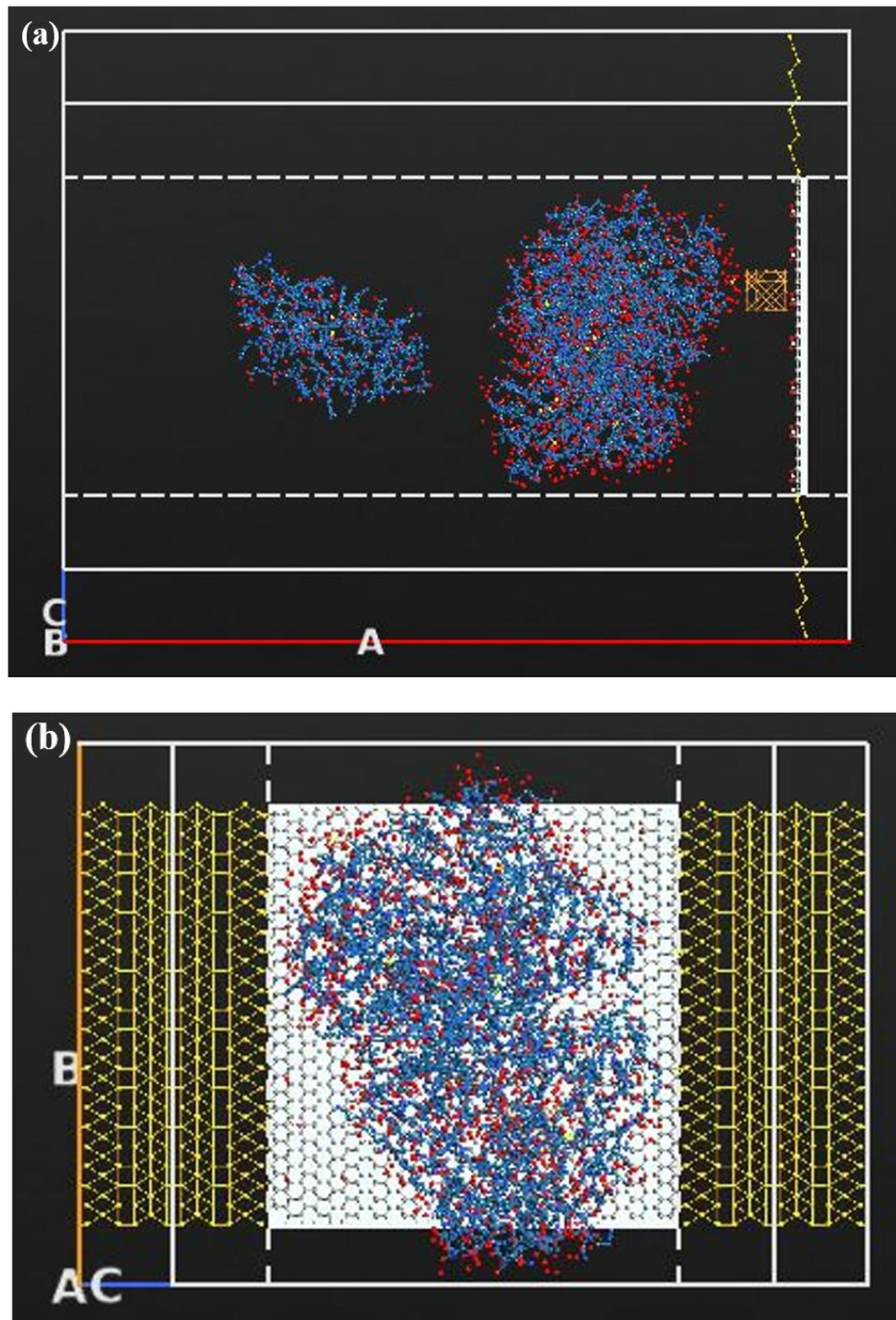
Figure 14: Different views of the sensor a) side and b) top views of the sensor with SARS-CoV-2 human neutralizing antibody, Cu MNPs and Rabies virus

3.5 Electrode-Channel Interface

A special plugin in the Quantum ATK software was used to create a stress free (relaxed) interfaces for our FET. It is crucial to have relaxed interfaces to build the design to avoid any effects on the electronic structures [126]. In this design we have two interfaces one on each side namely, golden left/right electrode – rGO channel. To understand the nature

of these interfaces and how ideal they are, the transmission spectrum figures for the mentioned interfaces were generated. It was confirmed that due to the continuous graphene nanoribbons down-sizing the contact resistance can dominate. This was attributed to the decreased number of available conduction modes [108]. However, to reduce this effect, end-contacted electrodes have been employed for the rGO-FET biosensor. Yuki's group [127] have shown that by using end contacted electrodes the resistance can be reduced by a factor reaching to ~7000. Another remarkable point is the interaction nature that occurs between the rGO channel and the metal electrode. This can go in two directions either physisorption or chemisorption, where the former doesn't introduce major electronic alteration, the latter does. Hence, gold was utilized as the electrode material in this design since it belongs to the physisorption family [63].

3.6 Semi-Empirical Model

Single atoms interactions are key points in having accurate results, thus it is very important to include these in the system's calculations. Recently, there have been several methods which are combined with the Nonequilibrium Green's Function (NEGF) formalism to perform these atomic scale calculations namely, ab initio approaches and Semi-Empirical (SE) approaches. Ab initio approach utilizes first principles such as Density Functional Theory (DFT) and have the advantage of predictive power with good results accuracy especially when there is no previous experimental data. Nevertheless, Kohn-Sham equations and one-particle states can introduce many issues in terms of insufficient description of the unoccupied energy levels and the need for parallel computers to perform the demanding calculations. Semi-Empirical approach is more suitable for our design since it has lower computational cost, can be fitted to experimental data and may also offer more accurate results. The NEGF formalism is employed in Quantumwise ATK software to carry out the non-equilibrium electron density calculations. The density matrix is divided into two terms namely, left and right as in below Equation:

$$D = D^L + D^R \quad [128] \qquad (1)$$

The contribution of the left density matrix is found by employing the NEGF using the following Equation:

$$D^L = \int \rho^L(\varepsilon) f\left(\frac{\varepsilon - \mu_L}{k_B T_L}\right) d\varepsilon, \qquad (2)$$

where the spectral density matrix is illustrated below:

$$\rho^L(\varepsilon) = \frac{1}{2\pi} G(\varepsilon) \Gamma^L(\varepsilon) G^+(\varepsilon) \qquad (3)$$

And the fermi function, electron temperature, retarded Green's function and left electrode's broadening function are shown as f, T_L, G, Γ^L respectively. Of course, a similar approach is followed for the right term as well [128]. Another interesting value known as the self energy which is a description of the impact the electrode states has on the central region's electronic structure, is calculated by the software, basically four methods are available namely, direct self energy [129], recursion self energy [130], Krylov self energy [131-132] and finally sparse recursion self energy which is employed in our design owing to its efficiency with large size systems [130].

There are several semiempirical transport models such as methods depending on Slater Koster (SK) tight-binding parameters and Extended Huckel (EH) parameters [133–135]. In the Self-Consistent (SC), SE designs in Quantumwise ATK the electron density causes a rise in the Hartree potential V_H which is included in the Hamiltonian as an additional term as shown in the following Equation:

$$H_{ij}^{SCF} = \frac{1}{2}(V_H(R_i) + V_H(R_j))S_{ij} \text{ [133]} \qquad (4)$$

Additionally, the occupied eigen functions are used to find the electron density as:

$$n(r) = \sum_\alpha f_\alpha |\psi_\alpha(r)|^2 \quad \text{[133]} \qquad (5)$$

where, α, f_α, ψ_α are the level, occupation of the level and eigenstate respectively.

In this work Extended Huckel (EH) parameters accompanied with Self-Consistent (SC) Hartree potential were used to carry out the system's study. Since a charge density needs to be generated a 10 Hartree mesh cut-off was fixed along all the device's calculations also a k-points grid of 3x3x68 for the Brillouin Zone is used. In order to have a zero derivative fixed electrostatic voltage, Poisson equation with conditional margins on the electrodes were employed such as, Dirichlet condition along C direction and Neumann boundary condition along A and B directions this was proved to be effective when

having a metal gate [136]. A combination of Hoffman and Cerda basis sets were applied on the carbon atoms in the system to reduce the computation time as possible while keeping a good accuracy. Hoffman basis set were applied on all other atoms [137]. The transmission spectrum was calculated in an energy range from -2 to 2 with 201 sampling points. To calculate the transmission between two electrodes (drain and source) under a certain applied voltage the following Equation was used:

$$T(E,V) = Tr[\Gamma_L(E,V)G(E,V)\Gamma_R(E,V)G(E,V)] \quad [138\text{-}139] \qquad (6)$$

where, the left and right electrodes coupling matrices are represented by $\Gamma_L(E,V)$ and $\Gamma_R(E,V)$ respectively and $G(E,V)$ is the device's active region Green's function. Moreover, transfer and output curves were generated from the final results in order to evaluate and study the sensor's performance. Additional information about graphene based FET sensor building and design in Quantumatk software can be found in this reference [140]. All simulations and studies have been conducted using Quantumwise Atomistix Tool Kit (ATK) with Virtual NanoLab package. The software allows the nano-scale studies by providing a graphical user interface known as Virtual Nano Lab (VNL). All simulations and runs was carried out with the help of a High Performance Computing environment (HPC) which has 232 high power computing machines. Each of these machines has 24 processing units and a memory of 48 GB. In this study, 2 computing nodes each with 36 cores were utilized in all of the simulations.

Chapter 4: Results and Discussions

In this chapter a study of the designed rGO-FET biosensor behavior is conducted. The change in the sensor's environment is reflected in its electrical measurements. Herein, we study the effects of these changes and how these can be used as detection evidence. The noticed alteration in the drain-source (I_{ds}) current at different bias (V_{ds}) voltages (0.1v, 0.2v, 0.3v) were used as inputs to draw output curves. Channel's transmission spectrum and its significance with regards to the channel's semiconducting nature is studied. Moreover, transfer curves of the bare sensor, the sensor with virus, and the sensor decorated with MNP's and virus are compared. Additionally, transmission spectrum with varied bias voltage (V_{ds}) are also presented and discussed. Finally, the sensor's output curves are generated with an overall performance evaluation.

4.1 Channel's Performance

The channel semiconducting nature was further confirmed from its zero bias transmission spectrum, the test was done on an energy interval of -2 to 2 with 201 energy points. The left and right electrodes were 8.42Å wide while the remaining 42.12Å were left for the central region (scattering region) as shown in Figure 15. It is evident from the rGO channel's transmission spectrum in Figure 16 that it has semiconducting properties due to the obvious 0.4 transmission bandgap below the fermi level (E_f). It can also be observed that the figure is asymmetric in the positive and negative regimes. This is because of the unique structure of the rGO which makes it non uniform since the oxygen functional groups are randomly scattered within it. This randomness can also cause an increased back scattering leading to a suppressed conductance [141]. Specifically, epoxies are the main reason of the broken symmetry between the holes and electrons close to the Dirac point [142]. Moreover, the covalent bonds between the graphene and the oxygen functional groups have a noticeable impact on the transmission spectrum which is apparent as conductance dips in the graph. It was proved that the sp^2 hybridization can be transformed into sp^3 hybridization as a result of covalent functionalization however this approach offers higher stability [99], [141]. Additionally, it can be noticed that there is a suppression in the valence band compared to the conduction band. This was attributed to the oxygen functional groups near the graphene

ribbon edges since their near-edge location leads to magnify the back scattering [141]. This suppression is expected to significantly increase when adding the metal electrodes owing to the interface's contact resistance.
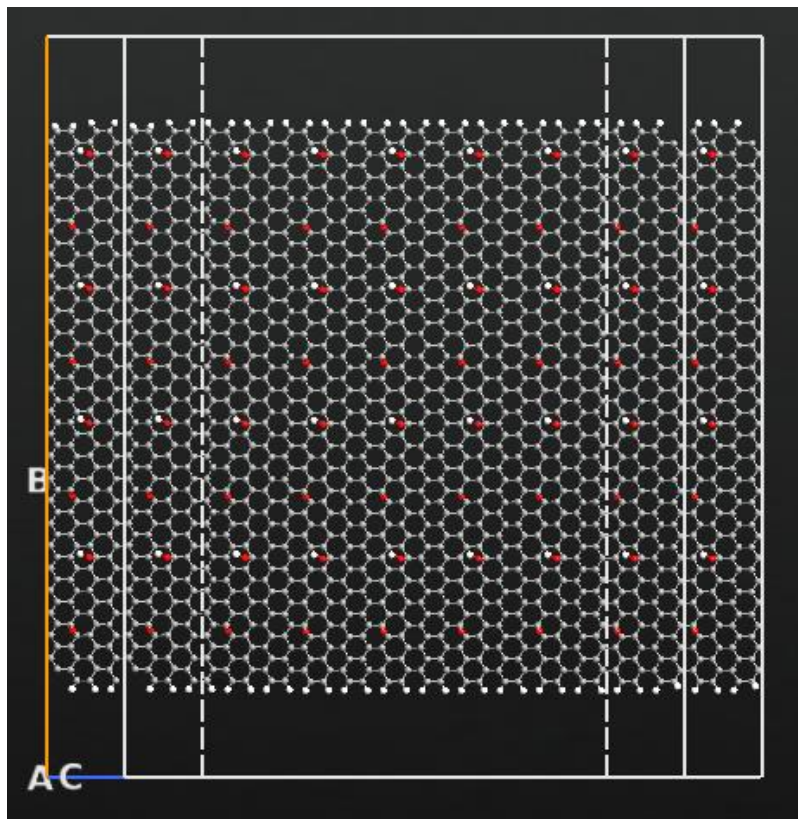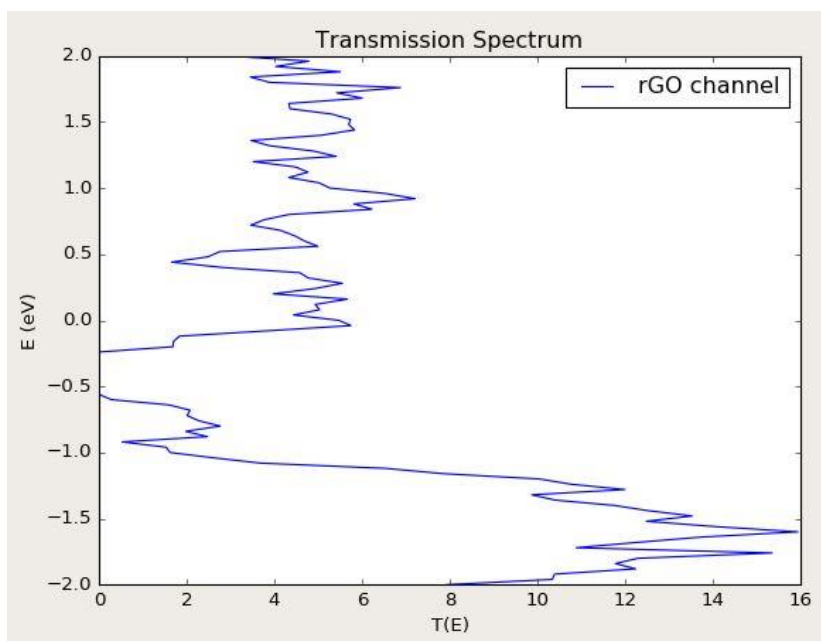

Figure 15: rGO channel testing structure

Figure 16: rGO channel's transmission spectrum

4.2 FET-Based Biosensor Performance

In this section, different electrical metrics are presented and used to study the biosensor's performance. Firstly, transmission spectrum of the whole system and the effect of adding the gold electrodes to our designed rGO channel is investigated. Secondly, the biosensors I-V characteristics curves are presented. Finally, the output curves are generated and compared (before and after the addition of the target molecules) for overall performance's evaluation. Most of the studies in literature has used changes in transfer curve as a target detection evidence, namely, change in CNP [90], [96], transconductance [143-144] (which is linear's section slope of the p- or n- branch in the transfer curve) and channel current [145]. Additionally, output curves were also employed to serve this matter just as presented in [91] and [139]. Herein, we keep an eye on transmission spectrums, transfer and output curve's changes and try to reach a unified conclusions on our design.

4.2.1 Biosensor's Characterization

The output (I_{ds}-V_{ds}) and transfer (I_{ds}-V_g) curves of the bare sensor are generated. It can be observed from the below output characteristic (Figure 17) that almost a linear relation in the biasing voltage range from 0 to 0.3 v at a gate voltage of 1 V is evidential, this apparent nonlinearity in the biosensor's behavior was attributed to the semiconductor (rGO channel) material which would result in a nonlinear I-V curve and hence a resistance nonlinearity [142-144]. Figure 17 shows that an ohmic contact between the rGO channel and the gold electrodes is obtained. Moreover, the drain source voltage was fixed at 0.05 v while sweeping the gate voltage between 0 and 0.4 v, the resulting transfer curve is shown in Figure 18. The curve exhibits an obvious v-shaped, ambipolar field effect transistor trend. The voltage at the minimum current value known as Dirac point is almost 0.2 v, this slightly positive shift in the Dirac point was attributed to some trapped impurities in the SiO_2 wafer below the rGO channel which causes intrinsic p-doping impact on the graphene [150].
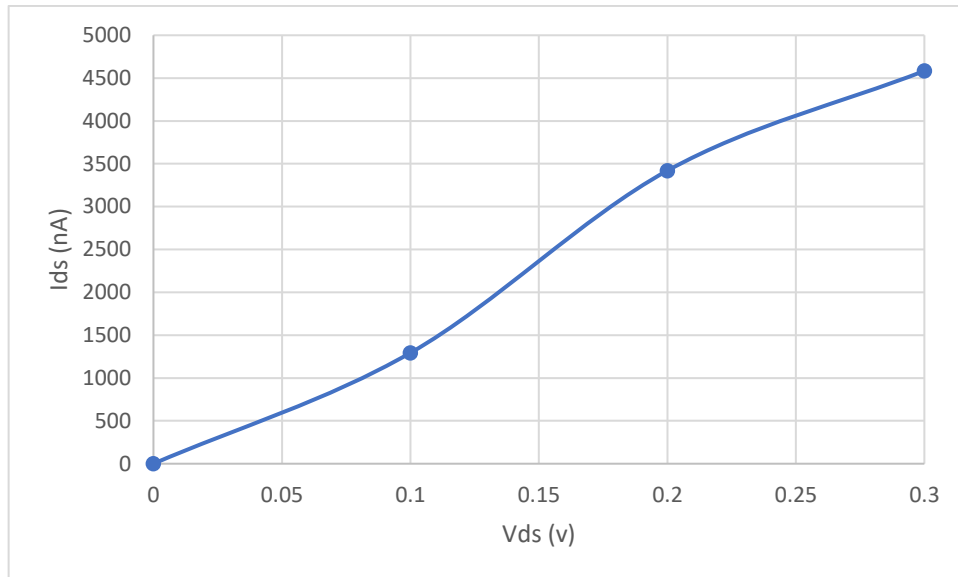
Figure 17: I-V curve of the bare G-FET sensor at V_g= 1 v
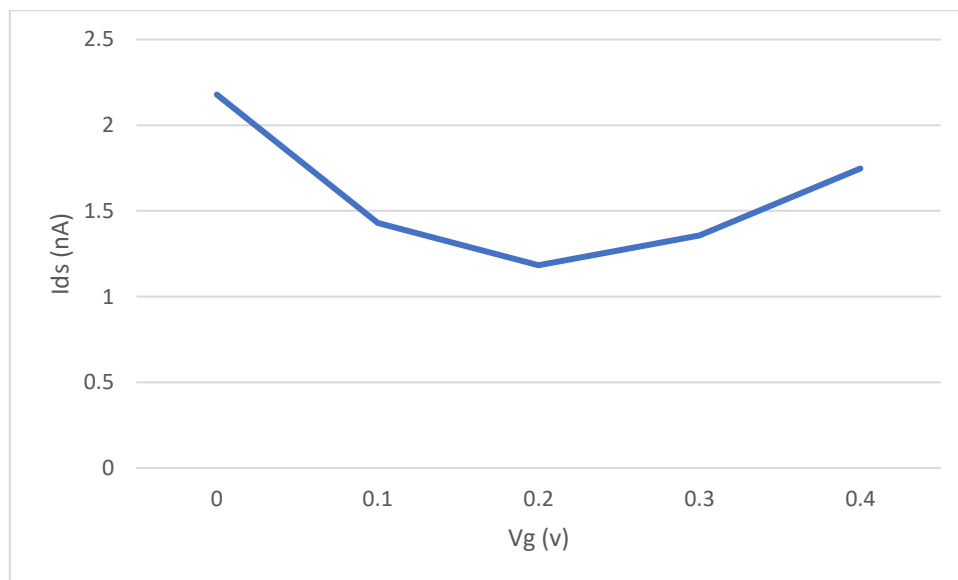
Figure 18: Transfer curve of the G-FET sensor at V_d=0.05 v

4.2.2 Biosensor's Transmission Spectrum

Transmission spectrum figures for the bare, virus, MNP's, and virus decorated sensor were produced for the bias voltages (V_{ds}) of 0.1, 0.2 and 0.3 volts. The spectrums are shown in Figures 19-22 below. At first glance, it can be seen that all of the spectrums exhibit an overall similar behavior that is suppressed valence band, multiple nonsymmetrical oscillations taking over most of the schemes, reduced transmission and diminishing, and moveable transport gap. Additionally, looking more closely at the

conduction band peak amplitude, we can notice that it slowly decreases with increasing applied voltage as follows, from 9 to 8 for bare sensor, from 8.6 to 8.1 for the virus-bound sensor, from 10.3 to 8.1 for the Cu MNPs decorated virus-bound sensor and from 7.9 to 7.2 for the Ag MNPs decorated virus-bound sensor. We have previously expected that transmission spectrum of the whole system will have a significant suppression in its valence band until reaching a full suppression in some positions. This demeanor can mainly be attributed to two main reasons: first, the near-edge positions of the functional oxygen groups which magnifies the back scattering and states' localization [141] and second, the addition of the gold electrodes or Metal Contacts (MC) that introduces an added contact resistance resulting in a decreased conductance. Contact resistance is actually one of the biggest challenges when designing a device based on a 2D material since a great portion of the applied bias is wasted by the parasitic resistance [108]. This phenomenon which is known as metallization can easily be spotted here. Regardless of the rising bias voltage there is no noticeable increase in transmission. Metallization effect caused by the gold MCs also introduces additional three major observations in our readings, primarily, the several little peaks that are apparent in each reading are normally a direct outcome of metallization. These peaks are known as Lorentzians [108]. According to Lorentz the force between an electron and atom's nucleus follows Hooke's law, also known as spring force. The existence of such force obliges the electrons to bear multiple oscillations caused by the electric field changes [151]. These oscillations are seen here as several little peaks. Secondly, metallization can also be observed from the unmistakably reduced transmission compared to the channel's before adding the MCs (from 16 to almost 9). The occurrence of Lorentzians and reduced conductance has been specifically attributed to the destructive interference impact on the travelling electrons along the FET which is the result of the constant broadening nature of the MCs [152]. Finally, transport gap is also affected by the MCs, as can be concluded from the spectrums, the gap has diminished, got significantly smaller (transmission less than 0.1) or changed its position in most of the cases. Poljak's group has related this manner to the rGO ribbon dimensions. They have concluded that the transport gap is strongly affected by the graphene ribbon width and length, while increasing the former leads to diminished gap, stretching the latter results in a broader one [108]. Apparently, from our

graphs it is obvious that the channel's width impact has dominated. Although the produced transmission figures reveal a similar pattern in general, they are also different, each one of them is unique and shows a singular response which will naturally lead to distinct current value for every case. This can be used as a detection evidence which will be further discussed in coming sections.
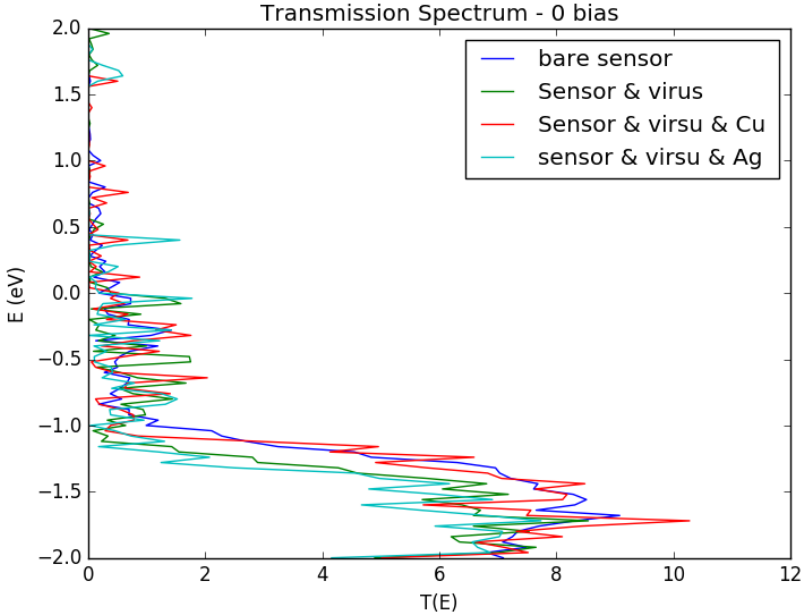
Figure 19: Transmission spectrum of the bare, virus bound, and MNPs decorated sensor at 0.0 bias voltage
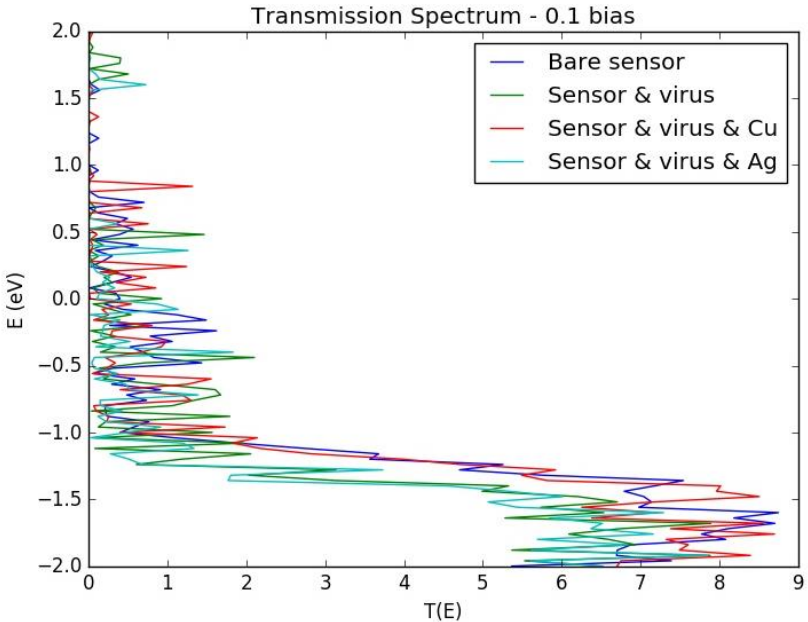
Figure 20: Transmission spectrum of the bare, virus bound, and MNPs decorated sensor at 0.1 bias voltage
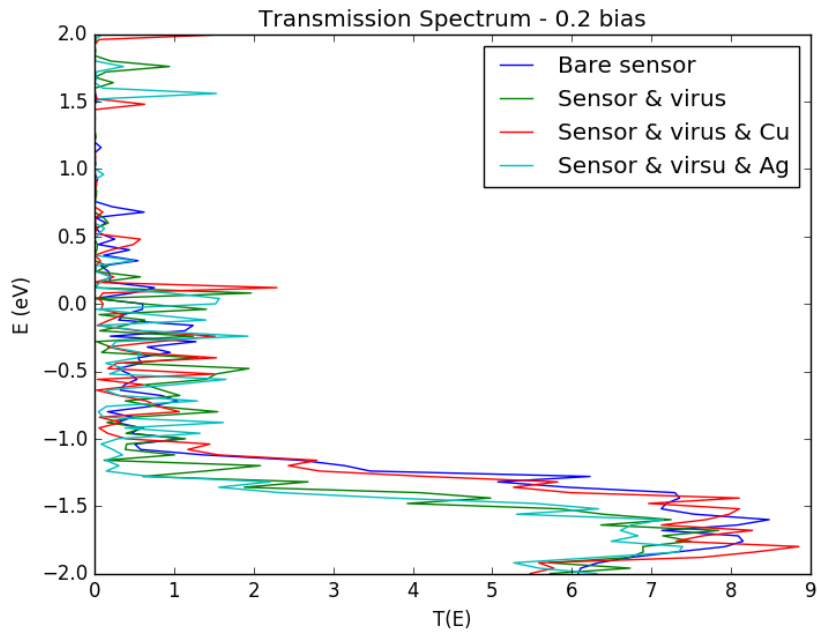
Figure 21: Transmission spectrum of the bare, virus bound, and MNPs decorated sensor at 0.2 bias voltage

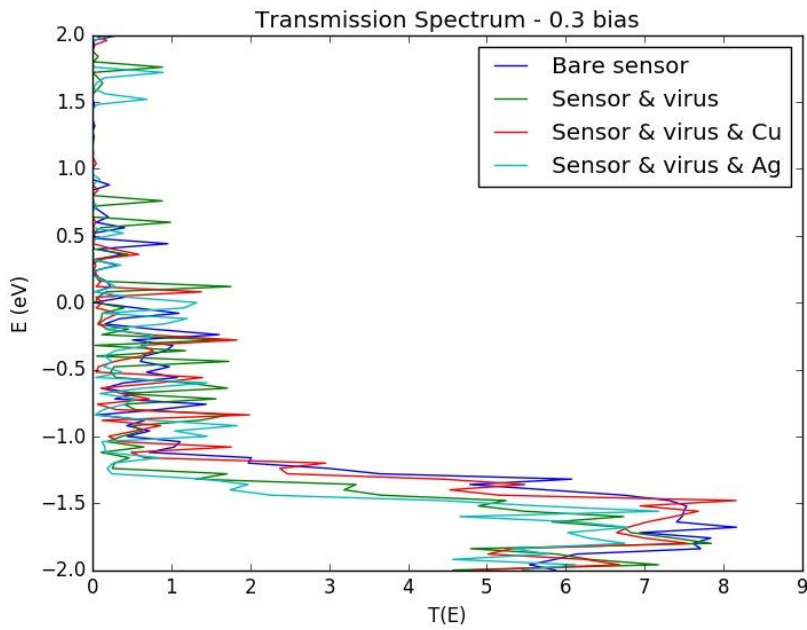Figure 22: Transmission spectrum of the bare, virus bound, and MNPs decorated sensor at 0.3 bias voltage

4.2.3 Biosensor's Output Curves

The biosensor's bias voltage (V_{ds}) versus the channel's current (I_{ds}) were plotted at a fixed gate voltage (V_g) of 1V to further study the sensor's performance. Figure 23 depicts the output curves of bare sensor, sensor with virus, and sensor decorated with

MNPs and virus. It is noticeable that the bare and virus and MNPs (Cu and Ag) functionalized cases show an almost linear relationship indicating an ohmic contact between the MCs and the rGO channel [36], [50]. On the contrary, the virus bound sensor shows a distinct Negative Differential Resistance (NDR) behavior, this result was anticipated for the reason that, MNPs' channel decoration was employed here to avoid the direct contact between the bio-target and the rGO channel since that can lead to altering the electronic structure of the rGO which eventually result in a distorted electrons distribution [112]. In Serhan's work, the NDR phenomenon was also linked to the coverage ratio, which is the percentage of carbon atoms having bonds with Oxygen functional groups in a specimen. He has concluded that rGO sheets with coverage ratios of 6.25 and 12.5% exhibit NDR behavior [153]. It is worth mentioning that our rGO channel has a coverage ratio of 11.2% which is very close to the ratios in the mentioned research. Obviously, functionalizing the rGO channel with MNPs has helped to eliminate NDR effect and enhance the sensor's bio-sensing performance. This definitely can be added to the list of advantages for using MNPs. Moreover, introducing Cu and Ag nanoparticles has firmly affected the sensor's I-V curve, the bare sensor had a current range between $1.293 - 4.585$ µA at V_{ds} ranging from 0 to 0.3 V and V_g of 1 V refer to blue line in the graph, while utilizing Cu atoms has lowered this range from 0.9713 to 3.290 µA (grey line) with same previous biasing and gate voltages conditions. Adding Ag atoms has unquestionably raised it to be from 1.581 to 7.880 µA (yellow line) keeping the same V_{ds} and V_g. These opposing trends were attributed to the charge carriers' movement between the introduced MNPs and the rGO sheet. It can be noticed that the movement was from the device's channel to the MNPs in the Cu atoms case while it was in the opposite direction in the Ag atoms situation. MNPs can either be acceptors (Cu in our case) or donors (Ag here) of charge carriers affecting the current value in the device [94]. These dramatic changes in the output curve from the reference case (bare sensor) can absolutely be used as a detection signal of our bio-target. Another important metric that can be used to measure the sensor's sensitivity is the current variation. Figure 24 depicts the current variations at different sensor's states. It can be seen that the current variation was the highest in the case of Ag MNP's decorated sensor. This leads to a very important conclusion which is, the silver nanoparticles show the best

performance and selectivity, since it introduces the largest variation in the drain current [147]. This exceptional behavior created by the Ag MNP's can be attributed to its interaction nature with the rGO channel as they act as charge carriers donors which eventually lead to electrical current increment [94].
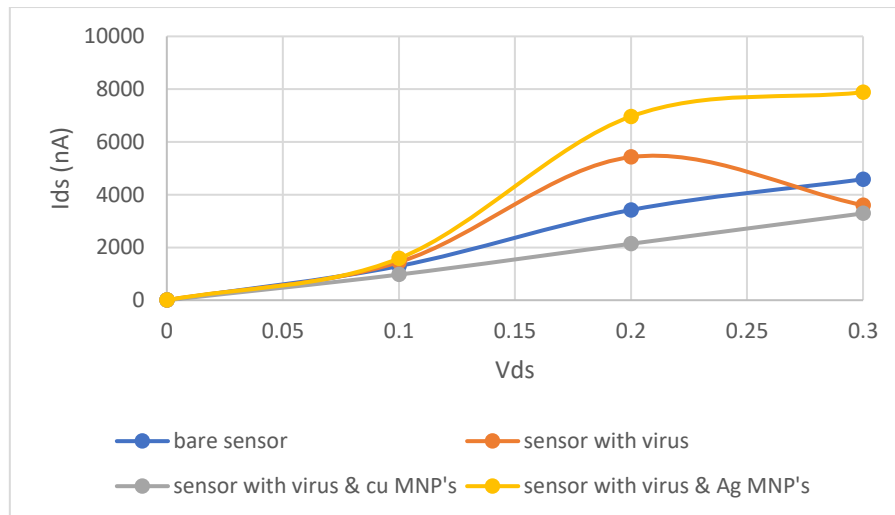
Figure 23: I-V curves of bare, virus-bound and MNPs decorated sensor at V_g= 1 V
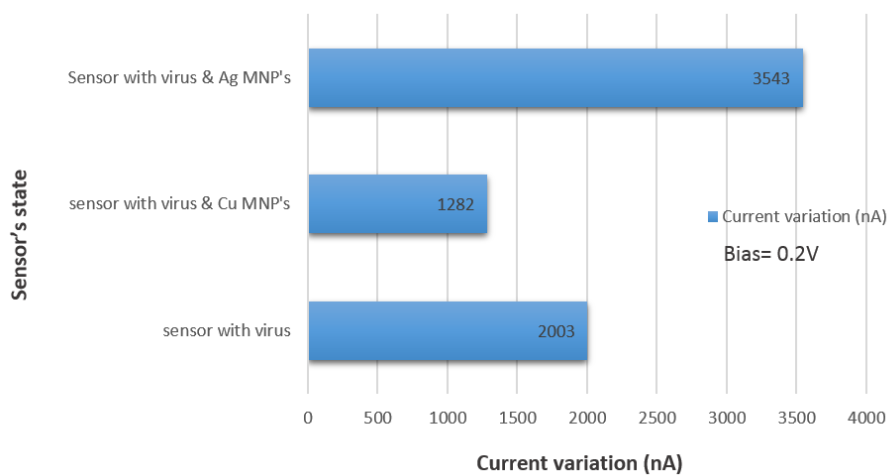
Figure 24: Current variation of the sensor with virus and MNP's decorated sensor

4.2.4 Biosensor's Selectivity

The sensor's specificity against other viruses such as Rabies virus was also tested. It can be noticed from Figure 25 below that no detectable change was spotted on the transmission spectrum by the software since the Rabies virus didn't bind to the

COVID-19 spike antibody. The spectrums here follow the same previously discussed trend with suppressed valence band and transmission reaching to maximum of 10. This work is a proof of concept that the designed rGO-FET biosensor could be used as a sensor for COVID-19 virus detection. The COVID-19 spike antibody was used to ensure the sensor accuracy and selectivity to the COVID-19 spike antigen. It is expected that the target molecules of COVID-19 spike antigen would bind to the COVID-19 spike antibodies, whereas the other viruses would not bind to the antibodies. A comparison of our design against other FET-based biosensors is illustrated in Table 3 below.
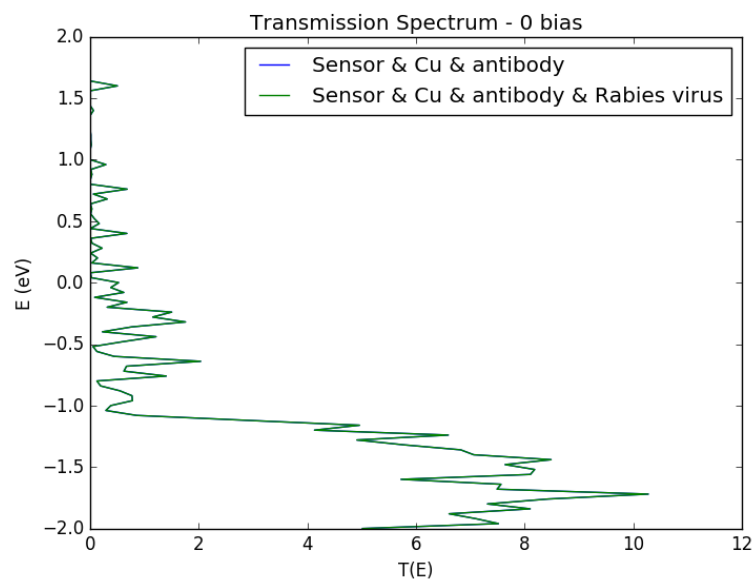
Figure 25: Transmission spectrums of SARS-CoV-2 human neutralizing antibody decorated sensors before and after addition of Rabies virus

Table 3: Comparison of our work and other rGO FETs biosensors.

Reference	Size	Target to be Detected	Channel Material
This work (simulation based)	8.274 x 6.124 nm^2	COVID-19 spike protein	rGO
[95] (fabrication)	6 x 4.5 mm^2	PNA-DNA hybridization	rGO
[50] (fabrication)	Sensing area= 100 x 100 μm^2	COVID-19 spike protein	rGO
[154] (simulation based)	Sensing area= 100 x 100 μm^2	Escherichia coli bacteria	graphene
[89] (fabrication)	Sensing area= 20 x 400 μm^2	PH sensing	rGO
[147] (simulation based)	Sensing area= 7.5 x 5.7 nm^2	COVID-19 spike protein	Silicon

Chapter 5: Conclusion and Future Works

In this thesis, we designed, studied and simulated an rGO Field Effect Transistor based biosensor to rapidly and accurately detect COVID-19 virus. The rGO was employed here as the detection site. The rGO channel was passivated with hydrogen at the edges. Moreover, the channel was decorated with metallic nanoparticles (copper and silver) and functionalized with SARS-CoV-2 human neutralizing antibody. All of these channel's preparation steps were very necessary to guarantee that the detection area is at its optimum detecting state and is suitable for bio-sensing applications. The rGO sheet was connected to gold electrodes to finally form the FET based biosensor. Gold was chosen since it doesn't introduce any major electronic alteration on the rGO channel. The whole arrangement was then tested using non-equilibrium Green's function method along with semiempirical approach namely, Extended Huckle. The self-consistent calculations revealed that the sensor is able to exhibit distinct results in each case. Various electronic transport characteristics such as: current, transmission spectrums and output curves were studied for the biosensor before and after viral exposure situations. The variations in the electronic characteristics due to the addition of the target molecule can be used as the bio-target detection signals. This work is a proof of concept that the designed rGO-FET biosensor could be used as a sensor for COVID-19 virus detection. The results indicated that the sensor showed a variation in current due to the COVID-19 spike protein in comparison to Rabies virus which didn't show any detection evidence. However, the fabrication process of such bio-sensors is expected to face some challenges such as the following:

- Fabrication of end contacted electrodes is a complex, time consuming and expensive process, however many researchers are studying alternative more efficient lithography approaches [1].
- Choosing the suitable molecular precursors to control the graphene nanoribbons structure since until recently it was a challenge to controllably fabricate graphene nanoribbons wider than n= 7 [2].
- RGO unified mass production has always been a challenge, since each sample of rGO has a unique electronic structure because oxygen functional groups scatters

randomly on the graphene surface meaning that no 100% identical samples can be produced which can affect the response of the sensor [3].

- Usage of real viral samples may affect the biosensor's sensitivity since it may cause many non-specific interactions [3].

In conclusion, this work is expected to aid in the on-going COVID-19 worldwide pandemic as it proposes an efficient, rapid, cost effective, and precise viral detection alternative.

References

[1]   B. Udugama, P. Kadhiresan, H. Kozlowski, A. Malekjahani, M. Osborne, V. Y C. Li, H. Chen, S. Mubareka, J. Gubbay, and W. Chan, "Diagnosing COVID-19: The Disease and Tools for Detection," *ACS Nano*, vol. 14, no. 4, pp. 3822–835, Apr. 2020, doi: 10.1021/acsnano.0c02624.

[2]   World Health Organization (WHO), "Coronavirus disease 2019 (COVID-19) situation report - 94," *World Health Organization*, Apr. 23, 2020. From: https://www.who.int/docs/default-source/coronaviruse/situation-reports/20200423-sitrep-94-covid-19.pdf?sfvrsn=b8304bf0_4 (accessed Sep. 20, 2021).

[3]   S. Chaplin, "COVID -19: a brief history and treatments in development," *Prescriber*, vol. 31, no. 5, pp. 23–28, May 2020, doi: 10.1002/psb.1843.

[4]   K. G. Andersen, A. Rambaut, W. I. Lipkin, E. C. Holmes, and R. F. Garry, "The proximal origin of SARS-CoV-2," *Nat. Med.*, vol. 26, no. 4, pp. 450–452, Apr. 2020, doi: 10.1038/s41591-020-0820-9.

[5]   J. Cui, F. Li, and Z.-L. Shi, "Origin and evolution of pathogenic coronaviruses," *Nat. Rev. Microbiol.*, vol. 17, no. 3, pp. 181–192, Mar. 2019, doi: 10.1038/s41579-018-0118-9.

[6]   X. Li, J. Zai, X. Wang, and Y. Li , "Potential of large 'first generation' human-to-human transmission of 2019-nCoV," *J. Med. Virol.*, vol. 92, no. 4, pp. 448–454, Apr. 2020. doi: 10.1002/jmv.25693.

[7]   G. J. Soufi, A. Hekmatnia, M. Nasrollahzadeh, and N. Shafiei, "SARS-CoV-2 (COVID-19): New Discoveries and Current Challenges," *Appl. Sci.*, vol. 10, no. 10, Art. no. 10, Jan. 2020, doi: 10.3390/app10103641.

[8]   M. Barcena, G. T. Oostergetel, W. Bartelink, F. G. A. Faas, A. Verkleij, P. J. M. Rottier, A. J. Koster, and B. J. Bosch, "Cryo-electron tomography of mouse hepatitis virus: Insights into the structure of the coronavirion," *Proc. Natl. Acad. Sci.*, vol. 106, no. 2, pp. 582–587, Jan. 2009, doi: 10.1073/pnas.0805270106.

[9]   S. Iravani, "Nano- and biosensors for the detection of SARS-CoV-2: challenges and opportunities," *Mater. Adv.*, vol. 1, no. 9, pp. 3092–3103, 2020, doi: 10.1039/D0MA00702A.

[10]   S. Boopathi, A. B. Poma, and P. Kolandaivel, "Novel 2019 coronavirus structure, mechanism of action, antiviral drug promises and rule out against its treatment," *J. Biomol. Struct. Dyn.*, pp. 1–10, Apr. 2020, doi: 10.1080/07391102.2020.1758788.

[11] M. Drobysh, A. Ramanaviciene, R. Viter, and A. Ramanavicius, "Affinity Sensors for the Diagnosis of COVID-19," *Micromachines*, vol. 12, no. 4, p. 390, Apr. 2021, doi: 10.3390/mi12040390.

[12] M. Cascella, M. Rajnik, A. Cuomo, S. C. Dulebohn, and R. Di Napoli, "Features, Evaluation, and Treatment of Coronavirus (COVID-19)," in *StatPearls*, Treasure Island (FL): StatPearls Publishing, 2020. [E-book] Available: http://www.ncbi.nlm.nih.gov/books/NBK554776/ (accessed Sep. 20, 2021).

[13] S .A. Deepak, K. R. Kottapalli, R. Rakwal, G. Oros, K. S. Rangappa, H. Iwahashi, Y. Masuo, and G. K. Agrawal, "Real-Time PCR: Revolutionizing Detection and Expression Analysis of Genes," *Curr. Genomics*, vol. 8, no. 4, pp. 234–251, Jun. 2007, doi: 10.2174/138920207781386960.

[14] A. Tahamtan and A. Ardebili, "Real-time RT-PCR in COVID-19 detection: issues affecting the results," *Expert Rev. Mol. Diagn.*, vol. 20, no. 5, pp. 453–454, May 2020, doi: 10.1080/14737159.2020.1757437.

[15] M. Karam, S. Althuwaikh, M. Alazemi, A. Abul, A. Hayre, A. Alsaif, and G. Barlow, "Chest CT versus RT-PCR for the detection of COVID-19: systematic review and meta-analysis of comparative studies," *JRSM Open*, vol. 12, no. 5, p. 20542704211011836, May 2021, doi: 10.1177/20542704211011837.

[16] S. Sheard, P. Rao, and A. Devaraj, "Imaging of acute respiratory distress syndrome," *Respir. Care*, vol. 57, no. 4, pp. 607–612, Apr. 2012, doi: 10.4187/respcare.01731.

[17] Z. Y. Zu, M. D. Jiang, P. P. Xu, W. Chen, Q. Q. Ni, G. M. Lu, and L. J. Zhang, "Coronavirus Disease 2019 (COVID-19): A Perspective from China," *Radiology*, vol. 296, no. 2, pp. E15–E25, Aug. 2020, doi: 10.1148/radiol.2020200490.

[18] M. Carotti, F. Salaffi, P. S. Puttini, A. Agostini, A. Borgheresi, D. Minorati, M. Galli, D. Marotto, and A. Giovagnoni, "Chest CT features of coronavirus disease 2019 (COVID-19) pneumonia: key points for radiologists," *Radiol. Med. (Torino)*, vol. 125, no. 7, pp. 636–646, Jul. 2020, doi: 10.1007/s11547-020-01237-4.

[19] A. Bernheim, X. Mei, M. Huang, Y. Yang, Z. A. Fayad, N. Zhang, K. Diao, B. Lin, X. Zhu, K. Li, S. Li, H. Shan, A. Jacobi, and M. Chung, "Chest CT Findings in Coronavirus Disease-19 (COVID-19): Relationship to Duration of Infection," *Radiology*, vol. 295, no. 3, p. 200463, Jun. 2020, doi: 10.1148/radiol.2020200463.

[20] Society of Thoracic Radiology, "Society of Thoracic Radiology. STR/ASER COVID-19 Position Statement," Mar. 11, 2020. From: https://thoracicrad.org/wp-content/uploads/2020/03/STR-ASER-Position-Statement-1.pdf (accessed Sep. 29, 2021).

[21] The Royal College of Radiologists, "The role of CT in patients suspected with COVID-19 infection: 12 March 2020, " From: https://www.rcr.ac.uk/posts/role-ct-patients-suspected-covid-19-infection-12-march-2020 (accessed Sep. 29, 2021).

[22] T. Ai, Z. Yang, H. Hou, C. Zhan, C. Chen, W. Lv, Q. Tao, Z. Sun, and L. Xia, "Correlation of Chest CT and RT-PCR Testing for Coronavirus Disease 2019 (COVID-19) in China: A Report of 1014 Cases," *Radiology*, vol. 296, no. 2, pp. E32–E40, Aug. 2020, doi: 10.1148/radiol.2020200642.

[23] N. Arora, A. K. Banerjee, and M. L. Narasu, "The role of artificial intelligence in tackling COVID-19," *Future Virol.*, vol. 15, no. 11, pp. 1-8 doi: 10.2217/fvl-2020-0130.

[24] T. Ozturk, M. Talo, E. A. Yildirim, U. B. Baloglu, O. Yildirim, and U. Rajendra Acharya, "Automated detection of COVID-19 cases using deep neural networks with X-ray images," *Comput. Biol. Med.*, vol. 121, p. 103792, Jun. 2020, doi: 10.1016/j.compbiomed.2020.103792.

[25] E. E.-D. Hemdan, M. A. Shouman, and M. E. Karar, "COVIDX-Net: A Framework of Deep Learning Classifiers to Diagnose COVID-19 in X-Ray Images," *ArXiv200311055 Cs Eess*, Mar. 2020. From: http://arxiv.org/abs/2003.11055 (accessed Sep. 29, 2021).

[26] H. Panwar, P. K. Gupta, M. K. Siddiqui, R. Morales-Menendez, and V. Singh, "Application of deep learning for fast detection of COVID-19 in X-Rays using nCOVnet," *Chaos Solitons Fractals*, vol. 138, p. 109944, Sep. 2020, doi: 10.1016/j.chaos.2020.109944.

[27] X. Zhu, X. Wang, L. Han, T. Chen, L. Wang, H. Li, S. Li, L. He, X. Fu, S. Chen, M. Xing, H. Chen, and Y. Wang, "Multiplex reverse transcription loop-mediated isothermal amplification combined with nanoparticle-based lateral flow biosensor for the diagnosis of COVID-19," *Biosens. Bioelectron.*, vol. 166, p. 112437, Oct. 2020, doi: 10.1016/j.bios.2020.112437.

[28] J. P. Broughton, X. Deng, G. Yu, C. L. Fasching, V. Servellita, J. Singh, X. Miao, J. A. Streithorst, A. Granados, A. S. Gonzalez, K. Zorn, A. Gopez, E. Hsu, W. Gu, S. Miller, C. Y. Pan, H. Guevara, D. A. Wadford, J. S. Chen, and C. Y. Chiu, "CRISPR–Cas12-based detection of SARS-CoV-2," *Nat. Biotechnol.*, vol. 38, no. 7, pp. 870–874, Jul. 2020, doi: 10.1038/s41587-020-0513-4.

[29] R. Samson, G. R. Navale, and M. S. Dharne, "Biosensors: frontiers in rapid detection of COVID-19," *3 Biotech*, vol. 10, no. 9, p. 385, Sep. 2020, doi: 10.1007/s13205-020-02369-0.

[30] T. Ozer, B. J. Geiss, and C. S. Henry, "Review—Chemical and Biological Sensors for Viral Detection," *J. Electrochem. Soc.*, vol. 167, no. 3, p. 037523, Jan. 2020, doi: 10.1149/2.0232003JES.

[31] K. Kerman, M. Kobayashi, and E. Tamiya, "Recent trends in electrochemical DNA biosensor technology," *Meas. Sci. Technol.*, vol. 15, no. 2, pp. R1–R11, Feb. 2004, doi: 10.1088/0957-0233/15/2/R01.

[32] H. Ilkhani and S. Farhad, "A novel electrochemical DNA biosensor for Ebola virus detection," *Anal. Biochem.*, vol. 557, pp. 151–155, Sep. 2018, doi: 10.1016/j.ab.2018.06.010.

[33] M. Manzano, S. Viezzi, S. Mazerat, R. S. Marks, and J. Vidic, "Rapid and label-free electrochemical DNA biosensor for detecting hepatitis A virus," *Biosens. Bioelectron.*, vol. 100, pp. 89–95, Feb. 2018, doi: 10.1016/j.bios.2017.08.043.

[34] G. Zhu, X. Yin, D. Jin, B. Zhang, Y. Gu, and Y. An, "Paper-based immunosensors: Current trends in the types and applied detection techniques," *TrAC Trends Anal. Chem.*, vol. 111, pp. 100–117, Feb. 2019, doi: 10.1016/j.trac.2018.09.027.

[35] Z. Zhang, Y. Cong, Y. Huang, and X. Du, "Nanomaterials-Based Electrochemical Immunosensors," *Micromachines*, vol. 10, no. 6, p. 397, Jun. 2019, doi: 10.3390/mi10060397.

[36] Y. Chen, R. Ren, H. Pu, X. Guo, J. Chang, G. Zhou, S. Mao, M. Kron, and J. Chen, "Field-Effect Transistor Biosensor for Rapid Detection of Ebola Antigen," *Sci. Rep.*, vol. 7, no. 1, p. 10974, Dec. 2017, doi: 10.1038/s41598-017-11387-7.

[37] Ü. Anik, Y. Tepeli, M. Sayhi, J. Nsiri, and M. F. Diouani, "Towards the electrochemical diagnostic of influenza virus: development of a graphene–Au hybrid nanocomposite modified influenza virus biosensor based on neuraminidase activity," *The Analyst*, vol. 143, no. 1, pp. 150–156, 2018, doi: 10.1039/C7AN01537B.

[38] T. Adachi and Y. Nakamura, "Aptamers: A Review of Their Chemical Properties and Modifications for Therapeutic Application," *Molecules*, vol. 24, no. 23, Nov. 2019, doi: 10.3390/molecules24234229.

[39] Y. Zhang, B. S. Lai, and M. Juhas, "Recent Advances in Aptamer Discovery and Applications," *Molecules*, vol. 24, no. 5, Mar. 2019, doi: 10.3390/molecules24050941.

[40] J. Lum, R. Wang, B. Hargis, S. Tung, W. Bottje, H. Lu, and Y. Li, "An Impedance Aptasensor with Microfluidic Chips for Specific Detection of H5N1 Avian Influenza Virus," *Sensors*, vol. 15, no. 8, pp. 18565–18578, Jul. 2015, doi: 10.3390/s150818565.

[41] C. Bai, Z. Lu, H. Jiang, Z. Yang, X. Liu, H. Ding, H. Li, J. Dong, A. Huang, T. Fang, Y. Jiang, L. Zhu, X. Lou, S. Li, and N. Shao, "Aptamer selection and application in multivalent binding-based electrical impedance detection of inactivated H1N1 virus," *Biosens. Bioelectron.*, vol. 110, pp. 162–167, Jul. 2018, doi: 10.1016/j.bios.2018.03.047.

[42] S. Sakamoto, W. Putalun, S. Vimolmangkang, W. Phoolcharoen, Y. Shoyama, H. Tanaka, and S. Morimoto, "Enzyme-linked immunosorbent assay for the quantitative/qualitative analysis of plant secondary metabolites," *J. Nat. Med.*, vol. 72, no. 1, pp. 32–42, Jan. 2018, doi: 10.1007/s11418-017-1144-z.

[43] S. Hosseini, P. Vázquez-Villegas, M. Rito-Palomares, and S. O. Martinez-Chapa, "Advantages, Disadvantages and Modifications of Conventional ELISA," in *Enzyme-linked Immunosorbent Assay (ELISA)*, Singapore: Springer Singapore, 2018, pp. 67–115. doi: 10.1007/978-981-10-6766-2_5.

[44] L. Wang, J. E. Filer, M. M. Lorenz, C. S. Henry, D. S. Dandy, and B. J. Geiss, "An ultra-sensitive capacitive microwire sensor for pathogen-specific serum antibody responses," *Biosens. Bioelectron.*, vol. 131, pp. 46–52, Apr. 2019, doi: 10.1016/j.bios.2019.01.040.

[45] J. L. Gogola, G. Martins, F. R. Caetano, T. R. Jorge, C. N. D. Santos, L. H. M. Junior, and M. F. Bergamini, "Label-free electrochemical immunosensor for quick detection of anti-hantavirus antibody," *J. Electroanal. Chem.*, vol. 842, pp. 140–145, Jun. 2019, doi: 10.1016/j.jelechem.2019.04.066.

[46] K.-H. Liang, T. J. Chang, M. L. Wang, P. H. Tsai, T. H. Lin, C. T. Wang, and D. M. Yang, "Novel biosensor platforms for the detection of coronavirus infection and severe acute respiratory syndrome coronavirus 2," *J. Chin. Med. Assoc.*, vol. 83, no. 8, pp. 701–703, Aug. 2020, doi: 10.1097/JCMA.0000000000000337.

[47] G. Binnig, H. Rohrer, C. Gerber, and E. Weibel, "Surface Studies by Scanning Tunneling Microscopy," *PRL*, vol. 49, p. 57, Jan. 1982, doi: 10.1007/978-94-011-1812-5_1.

[48] N. Chaniotakis and M. Fouskaki, "7 - Bio-chem-FETs: field effect transistors for biological sensing," in *Biological Identification*, R. P. Schaudies, Ed. Greece: Woodhead Publishing, 2014, pp. 194–219. doi: 10.1533/9780857099167.2.194.

[49] P. Fathi-Hafshejani, N. Azam, L. Wang, M. A. Kuroda, M. C. Hamilton, S. Hasim, and M. M. Samani, "Two-Dimensional-Material-Based Field-Effect Transistor Biosensor for Detecting COVID-19 Virus (SARS-CoV-2)," *ACS Nano*, vol. 15, no. 7, pp. 11461–11469, Jul. 2021, doi: 10.1021/acsnano.1c01188.

[50] G. Seo, G. Lee, M. J. Kim, S. H. Baek, M. Choi, K. B. Ku, C. S. Lee, S. Jun, D. Park, H. G. Kim, S. J. Kim, J. O. Lee, B. T. Kim, E. C. Park, and S. Kim, "Rapid Detection of COVID-19 Causative Virus (SARS-CoV-2) in Human Nasopharyngeal Swab Specimens Using Field-Effect Transistor-Based Biosensor," *ACS Nano*, vol. 14, no. 4, pp. 5135–5142, Apr. 2020, doi: 10.1021/acsnano.0c02823.

[51] C. Huang, T. Wen, F.-J. Shi, X.-Y. Zeng, and Y.-J. Jiao, "Rapid Detection of IgM Antibodies against the SARS-CoV-2 Virus via Colloidal Gold Nanoparticle-Based Lateral-Flow Assay," *ACS Omega*, vol. 5, no. 21, pp. 12550–12556, Jun. 2020, doi: 10.1021/acsomega.0c01554.

[52] S. Mahari, A. Roberts, D. Shahdeo, and S. Gandhi, "eCovSens-Ultrasensitive Novel In-House Built Printed Circuit Board Based Electrochemical Device for Rapid Detection of nCovid-19,*"bioRxiv,* Jan. 2020. doi: 10.1101/2020.04.24.059204.

[53] D. Bera, L. Qian, T.-K. Tseng, and P. H. Holloway, "Quantum Dots and Their Multimodal Applications: A Review," *Materials*, vol. 3, no. 4, pp. 2260–2345, Mar. 2010, doi: 10.3390/ma3042260.

[54] S. Şahin, C. Ünlü, and L. Trabzon, "Affinity biosensors developed with quantum dots in microfluidic systems," *Emergent Mater.*, pp. 1–23, Mar. 2021, doi: 10.1007/s42247-021-00195-5.

[55] G. Qiu, Z. Gai, Y. Tao, J. Schmitt, G. A. Kullak-Ublick, and J. Wang, "Dual-Functional Plasmonic Photothermal Biosensors for Highly Accurate Severe Acute Respiratory Syndrome Coronavirus 2 Detection," *ACS Nano*, vol. 14, no. 5, pp. 5268–5277, May 2020, doi: 10.1021/acsnano.0c02439.

[56] M. Zhang, X. Li, J. Pan, Y. Zhang, L. Zhang, C. Wang, X. Yan, X. Liu, and G. Lu, "Ultrasensitive detection of SARS-CoV-2 spike protein in untreated saliva using SERS-based biosensor," *Biosens. Bioelectron.*, vol. 190, p. 113421, Oct. 2021, doi: 10.1016/j.bios.2021.113421.

[57] A. H. Castro Neto, F. Guinea, N. M. R. Peres, K. S. Novoselov, and A. K. Geim, "The electronic properties of graphene," *Rev. Mod. Phys.*, vol. 81, no. 1, pp. 109–162, Jan. 2009, doi: 10.1103/RevModPhys.81.109.

[58] K. S. Novoselov, A. K. Geim, S.V. Morozov, D. Jiang, Y. Zhang, S. V. Dubonos, I. V. Grigorieva, and A. A. Firsov, "Electric Field Effect in Atomically Thin Carbon Films." *Science*, vol. 306, no. 5695, pp. 666-669, Oct. 2004, doi: 10.1126/science.1102986.

[59] A. Geim and A. Macdonald, "Graphene: Exploring carbon flatland" *Physics Today*, vol. 60, no. 8, Aug. 2007, doi: 10.1063/1.2774096.

[60] D. R. Cooper, B. D'Anjou, N. Ghattamaneni, and B. Harack, "Experimental Review of Graphene," *ISRN Condens. Matter Phys.*, vol. 2012, p. e501686, Apr. 2012, doi: 10.5402/2012/501686.

[61] S. Das Sarma, S. Adam, E. H. Hwang, and E. Rossi, "Electronic transport in two-dimensional graphene," *Rev. Mod. Phys.*, vol. 83, no. 2, pp. 407–470, May 2011, doi: 10.1103/RevModPhys.83.407.

[62] O. Klein, "Die Reflexion von Elektronen an einem Potentialsprung nach der relativistischen Dynamik von Dirac," *Z. F Phys.*, vol. 53, no. 3–4, pp. 157–165, Mar. 1929, doi: 10.1007/BF01339716.

[63] F. Giubileo and A. Di Bartolomeo, "The role of contact resistance in graphene field-effect devices," *Prog. Surf. Sci.*, vol. 92, no. 3, pp. 143–175, Aug. 2017, doi: 10.1016/j.progsurf.2017.05.002.

[64] H. Kroemer, "Quasi-electric and Quasi-Magnetic fields in Non-Uniform Semiconductors," *RCA Rev.*, vol. 18, pp. 332–342, 1957.

[65] M. Y. Han, B. Ozyilmaz, Y. Zhang, and P. Kim, "Energy band-gap engineering of graphene nanoribbons.," *Phys. Rev. Lett.*, 2007, doi: 10.1103/PhysRevLett.98.206805.

[66] E. V. Castro, K. S. Novoselov, S. V. Morozov, N. M. R. Peres, J. M. B. Lopes dos Santos, J. Nilsson, F. Guinea, A. K. Geim, and A. H. C. Neto, "Biased Bilayer Graphene: Semiconductor with a Gap Tunable by the Electric Field Effect," *Phys. Rev. Lett.*, vol. 99, no. 21, p. 216802, Nov. 2007, doi: 10.1103/PhysRevLett.99.216802.

[67] Y. Zhang, T. T. Tang, C. Girit, Z. Hao, M. C. Martin, A. Zettl, M. F. Crommie, Y. R. Shen, and F. Wang, "Direct observation of a widely tunable bandgap in bilayer graphene," *Nature*, vol. 459, no. 7248, pp. 820–823, Jun. 2009, doi: 10.1038/nature08105.

[68] G. Gui, J. Li, and J. Zhong, "Band structure engineering of graphene by strain: First-principles calculations," *Phys. Rev. B*, vol. 78, no. 7, p. 075435, Aug. 2008, doi: 10.1103/PhysRevB.78.075435.

[69] Y. Zhang, X. Wu, Q. Li, and J. Yang, "Tunable band gap of graphane nanoribbons under uniaxial elastic strain: a first-principles study," *arXiv labs,* Nov. 2011, From: https://arxiv.org/labs/1111/6336 (accessed Oct. 12, 2022).

[70] K. Vagdevi, V. Radhika Devi, and K. Venkateswara Rao, "First principles study of tunable band gap in bi layer Graphene (BLG)," *Mater. Today Proc.*, vol. 4, no. 8, pp. 7586–7591, Jan. 2017, doi: 10.1016/j.matpr.2017.07.091.

[71] H. Lee, K. Paeng, and I. S. Kim, "A review of doping modulation in graphene," *Synth. Met.*, vol. 244, pp. 36–47, Oct. 2018, doi: 10.1016/j.synthmet.2018.07.001.

[72] L. Liu and Z. Shen, "Bandgap engineering of graphene: A density functional theory study," *Appl. Phys. Lett.*, vol. 95, no. 25, p. 252104, Dec. 2009, doi: 10.1063/1.3276068.

[73] F. N. Ajeel, M. H. Mohammed, and A. M. Khudhair, "Energy bandgap engineering of graphene nanoribbon by doping phosphorous impurities to create nano-heterostructures: A DFT study," *Phys. E Low-Dimens. Syst. Nanostructures*, vol. 105, pp. 105–115, Jan. 2019, doi: 10.1016/j.physe.2018.09.006.

[74] H. Q. Ta, L. Zhao, W. Yin, D. Pohl, B. Rellinghaus, T. Gemming, B. Trzebicka, J. Palisaitis, G. Jing, P. O. A. Persson, Z. Liu, A. Bachmatiuk, and M. H. Rummeli, "Single Cr atom catalytic growth of graphene," *Nano Res.*, vol. 11, no. 5, pp. 2405–2411, May 2018, doi: 10.1007/s12274-017-1861-3.

[75] A. J. Marsden, P. Brommer, J. J. Mudd, and A. M. Dyson, "Effect of oxygen and nitrogen functionalization on the physical and electronic structure of graphene," *Nano Res.*, vol. 8, no. 8, pp. 2620–2635, Aug. 2015, doi: 10.1007/s12274-015-0768-0.

[76] R. Lv, G. Chen, Q. Li, A. McCreary, A. B. Mendez, S. V. Morozov, L. Liang, X. Declerck, N. P. Lopez, D. A. Cullen, S. Feng, A. L. Elias, R. C. Silva, K. Fujisawa, M. Endo, F. Kang, J. C. Charlier, V. Meunier, M. Pan, A. R. Harutyunyan, and K. S. Novoselov, and M. Terrones, "Ultrasensitive gas detection of large-area boron-doped graphene," *Proc. Natl. Acad. Sci. U. S. A.*, vol. 112, no. 47, pp. 14527–14532, Nov. 2015, doi: 10.1073/pnas.1505993112.

[77] F. Yavari, C. Kritzinger, C. Gaire, L. Song, H. Gulapalli, T. B. Tasciuc, P. M. Ajayan, and N. Koratkar, "Tunable Bandgap in Graphene by the Controlled Adsorption of Water Molecules," *Small*, vol. 6, no. 22, pp. 2535–2538, 2010, doi: 10.1002/smll.201001384.

[78] M. Acik and Y. Chabal, "A Review on Reducing Graphene Oxide for Band Gap Engineering," *J. Mater. Sci. Res.*, vol. 2, Oct. 2012, doi: 10.5539/jmsr.v2n1p101.

[79] Y. Jin, Y. Zheng, S. G. Podkolzin, and W. Lee, "Band gap of reduced graphene oxide tuned by controlling functional groups," *J. Mater. Chem. C*, vol. 8, no. 14, pp. 4885–4894, 2020, doi: 10.1039/C9TC07063J.

[80] J.-A. Yan and M. Y. Chou, "Oxidation functional groups on graphene: Structural and electronic properties," *Phys. Rev. B*, vol. 82, no. 12, p. 125403, Sep. 2010, doi: 10.1103/PhysRevB.82.125403.

[81] B. A. Arashloo, M. T. Ahmadi, and S. Afrang, "The band energy engineering on high epoxy (or hydroxyl) content graphene oxide," *Surf. Rev. Lett.*, vol. 26, no. 01, p. 1850135, Jan. 2019, doi: 10.1142/S0218625X18501354.

[82] S. D. Dabhi and P. K. Jha, "Tuning the electronic band gap of graphene by oxidation," *AIP Conf. Proc.*, vol. 1665, no. 1, p. 090013, Jun. 2015, doi: 10.1063/1.4917993.

[83] S. Rao, J. Upadhyay, K. Polychronopoulou, R. Umer, and R. Das, "Reduced Graphene Oxide: Effect of Reduction on Electrical Conductivity," *J. Compos. Sci.*, vol. 2, no. 2, p. 25, Apr. 2018, doi: 10.3390/jcs2020025.

[84] W. Liu and G. Speranza, "Tuning the Oxygen Content of Reduced Graphene Oxide and Effects on Its Properties," *ACS Omega*, vol. 6, no. 9, pp. 6195–6205, Mar. 2021, doi: 10.1021/acsomega.0c05578.

[85] H. A. Becerril, J. Mao, Z. Liu, R. M. Stoltenberg, Z. Bao, and Y. Chen, "Evaluation of Solution-Processed Reduced Graphene Oxide Films as Transparent Conductors," *ACS Nano*, vol. 2, no. 3, pp. 463–470, Mar. 2008, doi: 10.1021/nn700375n.

[86] P. Kumar, N. Divya, and J. K. Ratan, "Study on the physico-chemical properties of reduced graphene oxide with different degrees of reduction temperature," *J. Iran. Chem. Soc.*, vol. 18, no. 1, pp. 201–211, Jan. 2021, doi: 10.1007/s13738-020-02014-w.

[87] V. Tjoa, W. Jun, V. Dravid, S. Mhaisalkar, and N. Mathews, "Hybrid graphene–metal nanoparticle systems: electronic properties and gas interaction," *J. Mater. Chem.*, vol. 21, no. 39, p. 15593, 2011, doi: 10.1039/c1jm12676h.

[88] C. Yu, X. Chang, J. Liu, L. Ding, J. Peng, and Y. Fang, "Creation of Reduced Graphene Oxide Based Field Effect Transistors and Their Utilization in the Detection and Discrimination of Nucleoside Triphosphates," *ACS Appl. Mater. Interfaces*, vol. 7, no. 20, pp. 10718–10726, May 2015, doi: 10.1021/acsami.5b00155.

[89] I.-Y. Sohn, D. J. Kim, J. H. Jung, O. J. Yoon, T. N. Thanh, T. T. Quang, and N. E. Lee, "pH sensing characteristics and biosensing application of solution-gated reduced graphene oxide field-effect transistors," *Biosens. Bioelectron.*, vol. 45, pp. 70–76, Jul. 2013, doi: 10.1016/j.bios.2013.01.051.

[90] D.-J. Kim, I. Y. Sohn, J.-H. Jung, O. J. Yoon, N.-E. Lee, and J.-S. Park, "Reduced graphene oxide field-effect transistor for label-free femtomolar protein detection," *Biosens. Bioelectron.*, vol. 41, pp. 621–626, Mar. 2013, doi: 10.1016/j.bios.2012.09.040.

[91] P. Aspermair, V. Mishyn, J. Bintinger, H. Happy, K. Bagga, P. Subramanian, W. Knoll, R. Boukherroub, and S. Szunerits, "Reduced graphene oxide–based field effect transistors for the detection of E7 protein of human papillomavirus in saliva," *Anal. Bioanal. Chem.*, Aug. 2020, doi: 10.1007/s00216-020-02879-z.

[92] X. Jin, H. Zhang, Y. T. Li, M. M. Xiao, Z. L. Zhang, D. W. Pang, G. Wong, Z. Y. Zhang, and G. J. Zhang, "A field effect transistor modified with reduced graphene oxide for immunodetection of Ebola virus," *Microchim. Acta*, vol. 186, no. 4, p. 223, Apr. 2019, doi: 10.1007/s00604-019-3256-5.

[93] C. Chan, J. Shi, Y. Fan, and M. Yang, "A microfluidic flow-through chip integrated with reduced graphene oxide transistor for influenza virus gene detection," *Sens. Actuators B Chem.*, vol. 251, pp. 927–933, Nov. 2017, doi: 10.1016/j.snb.2017.05.147.

[94] M. H. Rashid, A. Koel, and T. Rang, "Simulations of Graphene Nanoribbon Field Effect Transistor for the Detection of Propane and Butane Gases: A First Principles Study," *Nanomaterials*, vol. 10, no. 1, p. 98, Jan. 2020, doi: 10.3390/nano10010098.

[95] B. Cai, S. Wang, L. Huang, Y. Ning, Z. Zhang, and G.-J. Zhang, "Ultrasensitive Label-Free Detection of PNA–DNA Hybridization by Reduced Graphene Oxide Field-Effect Transistor Biosensor," *ACS Nano*, vol. 8, no. 3, pp. 2632–2638, Mar. 2014, doi: 10.1021/nn4063424.

[96] G. Wu. Z. Dai, X. Tang, Z. Lin, P. K. Lo, M. Meyyappan, and K. W. C. Lai, "Graphene Field-Effect Transistors for the Sensitive and Selective Detection of Escherichia coli Using Pyrene-Tagged DNA Aptamer," *Adv. Healthc. Mater.*, vol. 6, no. 19, p. 1700736, Oct. 2017, doi: 10.1002/adhm.201700736.

[97] Synopsys, "Atomistic Simulation Software | QuantumATK - Synopsys." From: https://www.synopsys.com/silicon/quantumatk.html (accessed Oct. 12, 2021).

[98] C. Heitzinger, R. Kennell, G. Klimeck, N. Mauser, M. McLennan, and C. Ringhofer, "Modeling and simulation of field-effect biosensors (BioFETs) and their deployment on the nanoHUB," *J. Phys. Conf. Ser.*, vol. 107, p. 012004, Mar. 2008, doi: 10.1088/1742-6596/107/1/012004.

[99] A. Béraud, M. Sauvage, C. M. Bazán, M. Tie, A. Bencherif, and D. Bouilly, "Graphene field-effect transistors as bioanalytical sensors: design, operation and performance," *Analyst*, vol. 146, no. 2, pp. 403–428, Jan. 2021, doi: 10.1039/D0AN01661F.

[100] Z. Chen, A. Narita, and K. Müllen, "Graphene Nanoribbons: On-Surface Synthesis and Integration into Electronic Devices," *Adv. Mater.*, vol. 32, no. 45, p. 2001893, 2020, doi: 10.1002/adma.202001893.

[101] A. J. Way, E. A. Murray, F. Goltl, V. Saraswat, R. M. Jacobberger, M. Mavrikakis, and M. S. Arnold, "Anisotropic Synthesis of Armchair Graphene Nanoribbon Arrays from Sub-5 nm Seeds at Variable Pitches on Germanium," *J. Phys. Chem. Lett.*, vol. 10, no. 15, pp. 4266–4272, Aug. 2019, doi: 10.1021/acs.jpclett.9b01079.

[102] J. Sengupta and C. M. Hussain, "Graphene-based field-effect transistor biosensors for the rapid detection and analysis of viruses: A perspective in view of COVID-19," *Carbon Trends*, vol. 2, p. 100011, Jan. 2021, doi: 10.1016/j.cartre.2020.100011.

[103] M. M. Stylianakis, G. Viskadouros, C. Polyzoidis, G. Veisakis, G. Kenanakis, N. Kornilios, K. Petridis, and E. Kymakis, "Updating the Role of Reduced Graphene Oxide Ink on Field Emission Devices in Synergy with Charge Transfer Materials," *Nanomaterials*, vol. 9, no. 2, Art. no. 2, Feb. 2019, doi: 10.3390/nano9020137.

[104] J. F. Carneiro, M. J. Paulo, M. Siaj, A. C. Tavares, and M. R. V. Lanza, "Nb 2 O 5 nanoparticles supported on reduced graphene oxide sheets as electrocatalyst for the H 2 O 2 electrogeneration," *J. Catal.*, vol. 332, pp. 51–61, Dec. 2015, doi: 10.1016/j.jcat.2015.08.027.

[105] F. Lima, R. Alvim, and C. Miranda, "Selective dissociation of benzoic acid on carbonate surfaces: A density functional theory perspective," *Appl. Surf. Sci.*, vol. 529, p. 147103, Nov. 2020, doi: 10.1016/j.apsusc.2020.147103.

[106] B. Gupta, N. Kumar, K. Panda, V. Kanan, S. Joshi, and I. Visoly-Fisher, "Role of oxygen functional groups in reduced graphene oxide for lubrication," *Sci. Rep.*, vol. 7, no. 1, p. 45030, Mar. 2017, doi: 10.1038/srep45030.

[107] S. Mao, H. Pu, and J. Chen, "Graphene oxide and its reduction: modeling and experimental progress," *RSC Adv.*, vol. 2, no. 7, p. 2643, 2012, doi: 10.1039/c2ra00663d.

[108] M. Poljak and M. Matić, "Metallization-Induced Quantum Limits of Contact Resistance in Graphene Nanoribbons with One-Dimensional Contacts," *Materials*, vol. 14, no. 13, Art. no. 13, Jan. 2021, doi: 10.3390/ma14133670.

[109] R. Torres-Mendieta, D. Ventura-Espinosa, S. Sabater, J. Lancis, G. Mínguez-Vega, and J. A. Mata, "In situ decoration of graphene sheets with gold nanoparticles synthetized by pulsed laser ablation in liquids," *Sci. Rep.*, vol. 6, no. 1, p. 30478, Jul. 2016, doi: 10.1038/srep30478.

[110] S. He, K. K. Liu, S. Su, J. Yan, X. Mao, D. Wang, Y. He, L. J. Li, S. Song, and C. Fan, "Graphene-Based High-Efficiency Surface-Enhanced Raman Scattering-Active Platform for Sensitive and Multiplex DNA Detection," *Anal. Chem.*, vol. 84, no. 10, pp. 4622–4627, May 2012, doi: 10.1021/ac300577d.

[111] E. Jimenez-Cervantes, J. López-Barroso, A. L. Martínez-Hernández, and C. Velasco-Santos, "Graphene-Based Materials Functionalization with Natural Polymeric Biomolecules," in *Recent Advances in Graphene Research*, P. K. Nayak, Ed. Mexico: InTech, 2016. doi: 10.5772/64001.

[112] J. Park and M. Yan, "Covalent Functionalization of Graphene with Reactive Intermediates." *Acc. Chem. Res,* vol. 46, no. 1, pp. 181-189, Nov. 2012, doi: 101021/ar300172h

[113] A. Cordaro, G. Neri, M. T. Sciortino, A. Scala, and A. Piperno, "Graphene-Based Strategies in Liquid Biopsy and in Viral Diseases Diagnosis," *Nanomaterials*, vol. 10, no. 6, Art. no. 6, Jun. 2020, doi: 10.3390/nano10061014.

[114] Y. Gao, D. Xu, T. Cui, and D. Li, "Stability of hydrogen-terminated graphene edges," *Phys. Chem. Chem. Phys.*, vol. 23, no. 23, pp. 13261–13266, Jun. 2021, doi: 10.1039/D1CP01384J.

[115] Y. H. Lu, R. Q. Wu, L. Shen, M. Yang, Z. D. Sha, Y. Q. Cai, P. M. He, and Y. P. Feng, "Effects of edge passivation by hydrogen on electronic structure of armchair graphene nanoribbon and band gap engineering," *Appl. Phys. Lett.*, vol. 94, no. 12, p. 122111, Mar. 2009, doi: 10.1063/1.3103551.

[116] N. Poklonski, E. Kislyakov, S. Vyrko, O. Bubel, and S. Ratkevich, "Electronic band structure and magnetic states of zigzag graphene nanoribbons: Quantum chemical calculations," *J. Nanophotonics*, vol. 6, pp. 061712–1(9), Oct. 2012, doi: 10.1117/1.JNP.6.061712.

[117] B. Jmai, V. Silva, and P. M. Mendes, "2D Electronics Based on Graphene Field Effect Transistors: Tutorial for Modelling and Simulation," *Micromachines*, vol. 12, no. 8, p. 979, Aug. 2021, doi: 10.3390/mi12080979.

[118] M. C. Lemme, T. J. Echtermeyer, M. Baus, and H. Kurz, "A Graphene Field-Effect Device," *IEEE Electron Device Lett.*, vol. 28, no. 4, pp. 282–284, Apr. 2007, doi: 10.1109/LED.2007.891668.

[119] R. P. D. Bank, "RCSB PDB: Homepage." From: https://www.rcsb.org/ (accessed Oct. 18, 2021).

[120] R. P. D. Bank, "RCSB PDB - 6ZCZ: Crystal structure of receptor binding domain of SARS-CoV-2 Spike glycoprotein in ternary complex with EY6A Fab and a nanobody." From: https://www.rcsb.org/structure/6ZCZ (accessed Oct. 18, 2021).

[121] R. P. D. Bank, "RCSB PDB - 2IEQ: Core Structure of S2 from the Human Coronavirus NL63 Spike Glycoprotein." From: https://www.rcsb.org/structure/2IEQ (accessed Sep. 24, 2022).

[122] R.P.D. Bank, "RCSB PDB - 7BZ5: Structure of COVID-19 virus spike receptor-binding domain complexed with a neutralizing antibody." From: https://www.rcsb.org/structure/7bz5 (accessed Sep. 24, 2022).

[123] R. P. D. Bank, "RCSB PDB - 7C20: Crystal structure of Rabies virus (Nishigahara strain) phosphoprotein C-terminal domain (K214A)." From: https://www.rcsb.org/structure/7C20 (accessed Sep. 24, 2022).

[124] R. P. D. Bank, "RCSB PDB - 3RVC: Effector domain of NS1 from influenza A/PR/8/34 containing a W187A mutation." From: https://www.rcsb.org/structure/3RVC (accessed Nov. 17, 2021).

[125] R. P. D. Bank, "RCSB PDB - 7K8N: Crystal structure of an anti-SARS-CoV-2 human neutralizing antibody Fab fragment, C102." From: https://www.rcsb.org/structure/7K8N (accessed Nov. 17, 2021).

[126] QuantumATK, "Relaxation of devices using the OptimizeDeviceConfiguration study object | QuantumATK S-2021.06 Documentation." From: https://docs.quantumatk.com/tutorials/optimize_device_configuration/optimize_device_configuration.html (accessed Nov. 10, 2021).

[127] Y. Matsuda, W.-Q. Deng, and W. A. Goddard, "Contact Resistance for 'End-Contacted' Metal−Graphene and Metal−Nanotube Interfaces from Quantum Mechanics," *J. Phys. Chem. C*, vol. 114, no. 41, pp. 17845–17850, Oct. 2010, doi: 10.1021/jp806437y.

[128] T. Ozaki, K. Nishio, and H. Kino, "Efficient implementation of the nonequilibrium Green function method for electronic transport calculations," *Phys. Rev. B*, vol. 81, no. 3, p. 035116, Jan. 2010, doi: 10.1103/PhysRevB.81.035116.

[129] S. Sanvito, C. J. Lambert, J. H. Jefferson, and A. M. Bratkovsky, "General Green's-function formalism for transport calculations with spd Hamiltonians and giant magnetoresistance in Co- and Ni-based magnetic multilayers," *Phys. Rev. B*, vol. 59, no. 18, pp. 11936–11948, May 1999, doi: 10.1103/PhysRevB.59.11936.

[130] M. P. L. Sancho, J. M. L. Sancho, and J. Rubio "Highly convergent schemes for the calculation of bulk and surface Green functions" *Phys. F met. Phys.,* vol. 15, no. 4, p. 851, Nov. 2000, doi: 10.1088/0305-4608/15/4/009.

[131] H. H. B. Sørensen, P. C. Hansen, D. E. Petersen, S. Skelboe, and K. Stokbro, "Krylov subspace method for evaluating the self-energy matrices in electron transport calculations," *Phys. Rev. B*, vol. 77, no. 15, p. 155301, Apr. 2008, doi: 10.1103/PhysRevB.77.155301.

[132] H. H. B. Sørensen, P. C. Hansen, D. E. Petersen, S. Skelboe, and K. Stokbro, "Efficient wave-function matching approach for quantum transport calculations," *Phys. Rev. B*, vol. 79, no. 20, p. 205322, May 2009, doi: 10.1103/PhysRevB.79.205322.

[133] K. Stokbro, D. E. Petersen, S. Smidstrup, A. Blom, M. Ipsen, and K. Kaasbjerg, "Semiempirical model for nanoscale device simulations," *Phys. Rev. B*, vol. 82, no. 7, p. 075420, Aug. 2010, doi: 10.1103/PhysRevB.82.075420.

[134] A. K. Mukhopadhyay, and N. G. Mukherjee "Self-consistent methods in Hückel and extended Hückel theories." *Quantum Chemistry,* vol. 19, issue 4, Apr. 1981, doi: 10.1002/qua.560190405.

[135] M. Elstner, D. Porezag, G. Jungnickel, J. Elsner, M. Haugk, Th. Frauenheim, S. Suhai, and G. Seifert, "Self-consistent-charge density-functional tight-binding method for simulations of complex materials properties," *Phys. Rev. B*, vol. 58, no. 11, pp. 7260–7268, Sep. 1998, doi: 10.1103/PhysRevB.58.7260.

[136] V. Narendar, S. K. Gupta, and S. Saxena, "First Principle Study of Doped Graphene for FET Applications." *Silicon,* vol. 11, pp. 277–286, Feb. 2019, doi: 10.1006/s12633-018-9852-x.

[137] A. Wasfi, F. Awwad, and A. I. Ayesh, "Detection of DNA Bases via Field Effect Transistor of Graphene Nanoribbon with a Nanopore: Semi-empirical Modeling," *NanoBioscience*, vol. 21, issue 3, pp. 347–357, Jul. 2022, doi: 10.1109/TNB.2021.3077364.

[138] B. P. Pandey, "Transmission spectrum and *IV* characteristics of dual-gate Z-shaped graphene nanoribbon FET," *Nanomater. Energy*, vol. 7, no. 2, pp. 32–36, Dec. 2018, doi: 10.1680/jnaen.17.00013.

[139] Y. T. Yang, R. X. Ding, and J. X. Song, "Transport properties of boron-doped single-walled silicon carbide nanotubes," *Phys. B Condens. Matter*, vol. 406, no. 2, pp. 216–219, Jan. 2011, doi: 10.1016/j.physb.2010.10.046.

[140] QuantumATK, "Build a graphene nanoribbon transistor | QuantumATK S-2021.06 Documentation." From: https://docs.quantumatk.com/tutorials/quantumatk_graphene_transistor/quantumatk_graphene_transistor.html (accessed Dec. 05, 2021).

[141] A. Bezanilla, A. Cresti, B. Biel, J. Charlier, and S. Roche, "Quantum transport on graphene nanoribbons in the presence of disorder chapter 7," in *Graphene nanoribbons*. Spain: IOP Publishing Ltd, 2019, pp. 7–26, doi: 10.1088/978-0-7503-1701-6ch7.

[142] S. Roche, N. Leconte, F. Ortmann, A. Lherbier, D. Soriano, and J.-C. Charlier, "Quantum transport in disordered graphene: A theoretical perspective," *Solid State Commun.*, vol. 152, no. 15, pp. 1404–1410, Aug. 2012, doi: 10.1016/j.ssc.2012.04.030.

[143] C. Rozman, C. Kotlowski, and W. Knoll, "Electronic Biosensing with Functionalized rGO FETs." *Biosensors,* vol. 6, no 2, pp. 17, Apr. 2016, doi: 10.3390/bios6020017.

[144] C. Reiner-Rozman, M. Larisika, C. Nowak, and W. Knoll, "Graphene-based liquid-gated field effect transistor for biosensing: Theory and experiments," *Biosens. Bioelectron.*, vol. 70, pp. 21–27, Aug. 2015, doi: 10.1016/j.bios.2015.03.013.

[145] S. Farid, X. Meshik, M. Choi, S. Mukherjee, Y. Lan, D. Parikh, S. Poduri, U. Baterdene, C. Huang, Y. Y. Wang, P. Burke, M. Dutta, and M. A. Stroscio, "Detection of Interferon gamma using graphene and aptamer based FET-like electrochemical biosensor " *Biosensors and Bioelectronics,* vol. 71, pp. 294-299, Apr. 2015, doi: 10.1016/j.bios.2015.04.047.

[146] Y. Huang, X. Dong, Y. Liu, L.-J. Li, and P. Chen, "Graphene-based biosensors for detection of bacteria and their metabolic activities," *J. Mater. Chem.*, vol. 21, no. 33, pp. 12358–12362, Aug. 2011, doi: 10.1039/C1JM11436K.

[147] A. Wasfi, F. Awwad, J. G. Gelovani, N. Qamhieh, and A. I. Ayesh, "COVID-19 Detection via Silicon Nanowire Field-Effect Transistor: Setup and Modeling of Its Function," *Nanomaterials*, vol. 12, no. 15, p. 2638, Jul. 2022, doi: 10.3390/nano12152638.

[148] A. Wasfi, F. Awwad, N. Qamhieh, B. Al Murshidi, A. R. Palakkott, and J. G. Gelovani, "Real-time COVID-19 detection via graphite oxide-based field-effect transistor biosensors decorated with Pt/Pd nanoparticles," *Sci. Rep.*, vol. 12, p. 18155, Oct. 2022, doi: 10.1038/s41598-022-22249-2.

[149] B. Ibarlucea, L. Romhildt, F. Zorgiebel, and S. Pregl, "Gating Hysteresis as an Indicator for Silicon Nanowire FET Biosensors," *Appl. Sci.*, vol. 8, no. 6, Art. no. 6, Jun. 2018, doi: 10.3390/app8060950.

[150] K. Xu, X. Meshik, B. M. Nichols, E. Zakar, M. Dutta, and M. A. Stroscio, "Graphene- and aptamer-based electrochemical biosensor," *Nanotechnology*, vol. 25, no. 20, p. 205501, May 2014, doi: 10.1088/0957-4484/25/20/205501.

[151] MIT Open Courseware, "The Lorentz Oscillator and its Applications" From: https://ocw.mit.edu/courses/6-007-electromagnetic-energy-from-motors-to-lasers-spring-2011/resources/mit6_007s11_lorentz/ (accessed Jun. 17, 2022).

[152] D. Ryndyk, "*Theory of Quantum Transport at Nanoscale: An Introduction*," 1st ed. Switzerland: Springer, 2015. [E-book] Available: https://link.springer.com/book/10.1007/978-3-319-24088-6 (accessed Sep 23, 2022).

[153] S. Yamacli, "Voltage-Dependent Electronic Transport Properties of Reduced Graphene Oxide with Various Coverage Ratios," *Nano-Micro Lett.*, vol. 7, pp. 42–50, Oct. 2014, doi: 10.1007/s40820-014-0017-1.

[154] G. Wu, M. Meyyappan, and K. Lai, "Simulation of Graphene Field-Effect Transistor Biosensors for Bacterial Detection," *Sensors*, vol. 18, no. 6, p. 1715, May 2018, doi: 10.3390/s18061715.

UAE UNIVERSITY MASTER THESIS NO. 2022: 88

This work proposes and demonstrates a biosensor with reduced Graphene Oxide (rGO) based Field Effect Transistor (FET) for rapid and selective detection of Severe Acute Respiratory Syndrome Coronavirus 2 (SARS-CoV-2). The main objective of this thesis is to detect the SARS-CoV-2 spike protein antigen on spot selectively and rapidly.

Nisreen Alnaji received her Master of Science in Electrical Engineering from the Department of Electrical Engineering, College of Engineering at UAE University, UAE. She received her BSc in Electrical Engineering from the Alhijjawi College of Engineering, Yarmouk University, Jordan.

www.uaeu.ac.ae